RETURN-FROM-ORBIT SPACEPLANE CONFIGURATIONS WITH VARYING GEOMETRY, MISSIONS, AND PLANETARY ENVIRONMENTS

by

LEONARDO PIÑERO-PÉREZ

Presented to the Faculty of the Honors College of

The University of Texas at Arlington in Partial Fulfillment

of the Requirements

for the Degree of

HONORS BACHELOR OF SCIENCE IN AEROSPACE ENGINEERING

THE UNIVERSITY OF TEXAS AT ARLINGTON

August 2018

ACKNOWLEDGMENTS

Firstly, I would like to thank my faculty advisor, Dr. Bernd Chudoba, for his inspirational lectures and guidance throughout the latter half of my undergraduate education. Not only has his teaching improved my caliber as an engineer tremendously, but his candid outlook on how an individual can build their own future has motivated me to go further than I thought was possible. At this early of a stage in the design process that is my life, the tiniest of deviations have a large impact on the overall picture, and for that I am grateful.

I am grateful for the faculty, advisors, and staff at the Honors College and the Mechanical and Aerospace Engineering Department, who have given me a stellar education, a great community, and valuable skills to change the future.

I am immensely indebted to my parents for raising me to love learning and to strive for achievement, and to the rest of my family and friends for being understanding of my general unavailability these past few months and supportive of the work I do.

Thank you to Friedrich Nietzsche, whose works have provided the philosophical backbone for my ambition.

Lastly, and most importantly, I give thanks to my Creator for giving me and the rest of humanity the rational and creative faculties to impose our will onto the masterpiece that is the universe.

August 09, 2018

ABSTRACT

RETURN-FROM-ORBIT SPACEPLANE CONFIGURATIONS

WITH VARYING GEOMETRY, MISSIONS, AND

PLANETARY ENVIRONMENTS

Leonardo Piñero-Pérez, B.S. Aerospace Engineering

The University of Texas at Arlington, 2018

Faculty Mentor: Bernd Chudoba

This thesis intends to remove underlying conceptual assumptions for spacecraft design and build a parameterized, physics-based approach based on geometry to generate a continuum of re-entry vehicle configurations. These vehicle configurations are then assessed by their payload, orbital and atmospheric maneuvering, and descent performance capabilities. This assessment is designed such that different missions on different planetary bodies can be analyzed.

In addition to selected historical configurations, the specific geometric parameters are then analyzed to determine how specific changes in certain parameters affect aircraft performance. In this way, the values for basic vehicle geometry can be selected in the proper combination to form the best configuration for a given mission.

Lastly, a regression methodology is established to use this physics-based model to converge on optimal designs initialized by selected point configurations.

TABLE OF CONTENTS

ACKNOWLEDGMENTS iii

ABSTRACT.. iv

LIST OF ILLUSTRATIONS.. ix

LIST OF TABLES xiii

Chapter

1. INTRODUCTION 1

1.1 Relevance of Thesis 1

1.1.1 Applicability to Industry 1

1.1.2 Applicability to Senior Project.. 2

1.2 Overview of Senior Project.. 2

1.2.1 Global Context 2

1.2.2 Expectations and Team Organization 7

1.2.3 Roles of Author in Team.. 10

1.2.4 Business Case.. 10

1.2.5 Model 176 Mission Profile 17

2. LITERATURE REVIEW 21

2.1 Historical Spacecraft 21

2.1.1 Capsule Vehicles.. 21

2.1.2 Wing-Body Vehicles... 23

2.1.3 Lifting-Body Vehicles 25

2.2 Background Material for Implemented Methods 28

2.2.1 Vehicle Environment 28

2.2.2 Vehicle Flight Path and Loads 30

2.2.3 Vehicle Design Parameters 33

3. METHODOLOGY 34

3.1 Geometry Definition 34

3.1.1 Parameters Chosen 34

3.1.2 Superimposed Wing 38

3.1.3 Historical Validation of Geometry 40

3.2 Geometry Analysis 42

3.2.1 Planform Area 42

3.2.2 Wetted Area 43

3.2.3 Volume 44

3.2.4 Küchemann's Tau 45

3.3 Vehicle Analysis 45

3.3.1 Structural Weight 45

3.3.2 Propulsion System 45

3.3.3 Delta V 46

3.3.4 Lift to Drag Ratio 47

3.4 Performance Analysis 48

3.4.1 Payload Capability 48

3.4.2 Synergetic Maneuver 49

3.4.3 Descent Trajectory 53

3.4.4 Total Performance 56

4. APPLICATION 57

4.1 Code Architecture 57

4.1.1 User Settings 57

4.1.2 Assessment 58

4.1.3 Full Process 59

4.2 Results and Comparisons 60

4.2.1 Trends in Geometry 60

4.2.2 Data Points 67

4.2.3 Historical Designs 68

4.3 Optimization 68

4.3.1 Methodology 68

4.3.2 Results 70

4.3.3 Observations 77

5. CONCLUSION 78

5.1 Concluding Remarks 78

5.2 Future Work 79

Appendix

A. NOMENCLATURE 81

REFERENCES 86

BIOGRAPHICAL INFORMATION 90

LIST OF ILLUSTRATIONS

Figure		Page
1.1	Flight Profile of the Synergetic Maneuver	4
1.2	Comparison of Systems for ΔV Required to Change Orbital Inclination	5
1.3	Payload Cost Per Pound vs. Flight Frequency	6
1.4	Space Activity After Lower Launch Costs from Operational Flexibility	6
1.5	Comparative Configurations for Hypersonic Re-entry Vehicles	8
1.6	Team Structure for Senior Project	9
1.7	Existing Launch Sites and Planned Launch Sites for Point-to-Point Transport	12
1.8	Interior Layout of Civilian Variant of the Model 176	13
1.9	Revenues and Costs as a Function of Flight Rate	15
1.10	Lateral Range Capability and Inclination's Effects on Orbital Wait Time	16
1.11	Expected Fleet Size (Left to Right): Civilian PtP, C&C, and Reconnaissance	17
1.12	Point-to-Point Variant Upper Stage Mission Diagram	17
1.13	Command-and-Control Variant Mission Profile	19
1.14	Reconnaissance Variant Upper Stage Mission Profile	20
2.1	Diagram of Apollo Re-entry Capsule (doubles as Command Module)	22
2.2	The Silber Vogel as Imagined in the Amerika Bomber Program	24
2.3	Generalized Mission Profile of the Silber Vogel (Dynamic Soaring)	25

2.4 Different Types of Lifting Body Vehicles (M1-L circled) 26

2.5 Evolution of Lifting Body Vehicles 27

2.6 Wrapping the X-24B Geometry around the X-24A...................................... 27

2.7 Region of Flight where Chapman's Analysis is Significant 30

3.1 Different Historical Configurations must be able to Relate on a Continuum.. 34

3.2 Spherical Spacecraft Design as a Re-entry Aircraft 35

3.3 New Generalized Design Now defined by Chord and Radius...................... 36

3.4 Generalized Design after Unlocking the Equal Radii Constraint 37

3.5 General Design Described by Nose and Aft Radii, Chord, and Span........... 38

3.6 Generalized Fuselage with a Superimposed Generalized Delta Wing 39

3.7 X-20 Dyna Soar Represented by Geometric Parameters.............................. 40

3.8 Mercury Capsule Represented by Geometric Parameters 41

3.9 Model 176 Represented by Geometric Parameters....................................... 42

3.10 Volume Breakdown for First-Order Vehicle 46

3.11 Alternative Lift-to-Drag Ratio Estimation Method from Tau 48

3.12 Synergetic Maneuver for a 45-degree Turn-Cone Angle 49

3.13 Lift-to-Drag Ratio Effect on Expended ΔV for an Earth Inclination Change 52

3.14 Synergetic Maneuvering Requirements on Mars.. 52

3.15 Vehicle Descent Range as a Function of Tau 54

3.16 Steady Glides for Differing Vehicle Parameters 55

3.17 Aerodynamic Load Factor with Fixed Vehicle Parameters.......................... 55

3.18 User-specified Weights define Mission Priorities 56

4.1	Four Parameters Describing the Planetary Environment	57
4.2	Four Parameters Describing the Desired Mission	58
4.3	Nassi-Schneiderman Diagram of Code Architecture	60
4.4	Adjusting Values of Chord and Span to View Trends	61
4.5	Wetted Area after Adjusting Span and Chord	61
4.6	Structural Weight after Adjusting Span and Chord	62
4.7	Küchemann's Tau after Adjusting Span and Chord	63
4.8	Available Volume after Adjusting Span and Chord	63
4.9	Adjusting Nose Radius to View Trends	64
4.10	Changing Parameters after Adjusting Nose Radius	64
4.11	Changing Parameters after Adjusting Chord	65
4.12	Inclination Change Capability with Increasing Chord	66
4.13	Genealogy of Configurations	69
4.14	Topology Visualized in Optimization Routine	70
4.15	Generation 1 of First Successful Convergence	71
4.16	Generation 900 with Improved Performance	71
4.17	Generation 1600 with Improved Aerodynamic and Payload Capability	72
4.18	Generation 3000 Lacks Propulsive Capability to Increase Payload Capability	73
4.19	Vehicle Evolution for First Successful Convergence	73
4.20	Vehicle Parameter Evolution for First Successful Convergence	74
4.21	Convergence to Mission Failure where Aerodynamic Capability is too High	75
4.22	Convergence to a Capsule with a Lifting Capability using New L/D Estimate	75

4.23 Geometric Evolution of Second Converged Configuration 76

4.24 Vehicle Parameters in Second Converged Configuration 76

4.25 Growing Nose due to Structural Weight Calculation Mistake 77

LIST OF TABLES

Table Page

1.1 US and Global Demand for Orbital Transportation 14

1.2 Infrastructure Costs as a Function of Flight Rate 14

2.1 Physical Data of Planets of Interest and Moon 29

2.2 Solutions for Z Based on Vehicle Type 31

CHAPTER 1

INTRODUCTION

1.1 Relevance of Thesis

1.1.1 Applicability to Industry

The main theme of this thesis is to remove underlying conceptual assumptions for spacecraft design and build a parameterized, physics-based approach to unique vehicle design. In this way, the values for basic vehicle geometry can be selected in the proper combination to form the best configuration for a given mission. The focus of this thesis involves the configuration's atmospheric performance for synergetic maneuvers and re-entry. The desired mission characteristics include inclination change and payload capability for a given vehicle weight.

The environments of other planetary bodies' atmospheres do not have a history of design predecessors to draw from. Even for special Earth-orbital missions, such as radically changing orbital inclination by means of a lifting body, there are little to no historical precedents from which a conceptual design can begin. If a designer is to make an educated conceptual decision, all possible configurations must be assessed. For this reason, the author proposes building a multi-dimensional topology of possible designs based on basic geometry for a given mission and its environment.

Such a tool should not only accurately assess existing designs but should also be predictive in determining possible configurations for novel missions, most interestingly for a new planetary environment. Many of the challenges of human spaceflight are not from a lack of technology, but rather from the lack of implementing holistic synthesis strategies to arrive at an optimum multi-disciplinary design point to maximize performance. The goal of this thesis is to provide insight into surmounting the latter challenge with existing technology.

1.1.2 Applicability to Senior Project

The author's senior project focused on a high-performing lifting body design which will serve as a test point for validating the methodologies of this thesis. Additionally, the analysis methodology uses the geometry of the vehicle as an input, and the results found from these analyses will be part of the core processes of the code developed by the author. The results of the senior project also provide context for the development of a business case and global impact of vehicles with one of the key performance parameters: cross-range. This performance parameter is a component in the overall performance of several vehicles, both historical and hypothetical.

The next section will go over the main findings and implications of the mission and design of the project's studied vehicle. The mission type and performance parameters involved in the senior project correlate to the assessment of vehicles in this thesis.

1.2 Overview of Senior Project

1.2.1 Global Context

This honors thesis is built upon the work from the author's senior design project, which is to re-create and document the conceptual design process for a lifting-body return-from-orbit vehicle and its associated reusable launch platform. The senior project was conducted by Ascension Aerospace, which is a team composed of 21 undergraduate senior-level aerospace engineering students. This group project is the main deliverable for the MAE 4351 Capstone Design Course at the University of Texas at Arlington, Texas. The author's role in this class team is that of the lead chief engineer. Much of the first chapter in this thesis is adapted from the author's senior project report.

At the time of the writing of this thesis, the United States is falling behind in space warfare, and there has been renewed interest in the rapid development of hypersonic vehicles to counteract Russian and Chinese military strategy. This geopolitical situation is exemplified by United States President Donald Trump's June 18th 2018 declaration, directing the department of defense and pentagon to initiate a sixth branch of the American armed forces, known as the "Space Force" [4]. This new initiative has the intent of increasing American military readiness and dominance within Earth's orbital sphere-of-influence and beyond. Hypersonic vehicle development is an essential element of such an initiative. The generation of high-performing vehicle concepts for hypersonic flight is the focus of this thesis.

One useful application of a high-lift hypersonic craft is the ability to rapidly change the orbital inclination by descending from orbit into a hypersonic upper-atmospheric flight regime and using aerodynamic effectors to alter the trajectory. The spacecraft would then emerge into an exoatmospheric orbit at a new inclination accompanied by radically improved surface coverage.

This application allows for surprise reconnaissance, which a purely orbital satellite is incapable of doing without expending copious amounts of fuel by chemical combustion. By utilizing a hypersonic reconnaissance vehicle, the operator has complete flexibility in major course corrections, which is especially useful for fast-paced, unpredictable military missions. Figure 1.2 roughly compares the performance of a high-lift vehicle such as the McDonnel Model 176 (the focus vehicle of senior project) and a conventional satellite which is required by its mission to change inclination. The current situation only permits predictable spy-satellite orbits which potentially allows an enemy to effectively hide operations and wait for the known spy-satellite to complete its overhead pass. With a maneuver synergetic with the aerodynamic properties of a specialized vehicle such as the Model 176 (focus of the senior project and a vehicle study in this thesis), the military can now utilize a high-inclination change missions originating from orbit. Additionally, a high cross-range capability is desired so that orbit time can be reduced, allowing the military craft to return to friendly territory (continental United States) at a moment's notice. The mission profile of this craft's synergetic maneuver can be generalized as shown in Figure 1.1 (adapted from [2]).

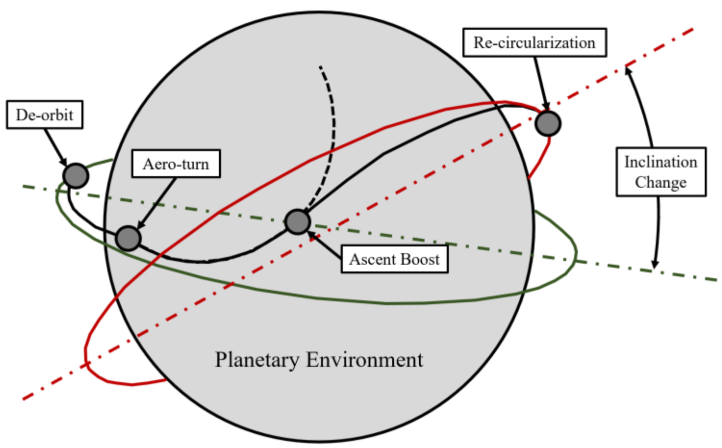

Figure 1.1: Flight Profile of the Synergetic Maneuver

Later in this thesis, this comparison will be studied in greater detail to find how geometry affects the inclination-change performance. Vehicles of identical geometry will defer in performance as a function of planetary environment or method of inclination change (using either a synergetic maneuver or a purely propulsive system).

As shown, it is not feasible to carry the necessary fuel to make large changes in inclination by conventional propulsive means. It is worth noting that that conventional inclination changes are actually advantageous for lower inclination changes since the initial fuel cost is zero. A synergetic mission profile requires multiple burns to descend into the upper atmosphere and ascend into the new orbit [6].

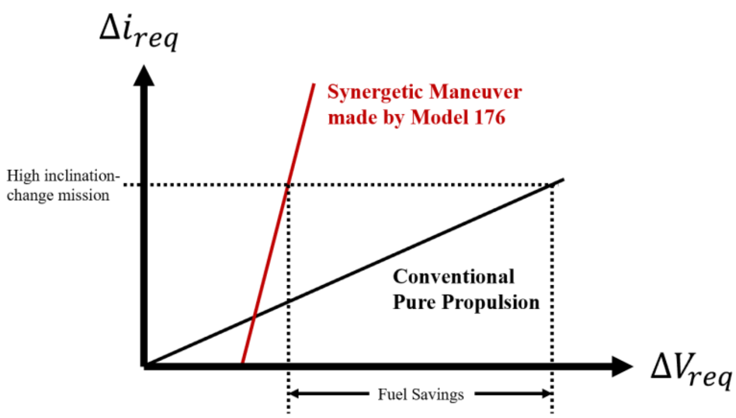

Figure 1.2: Comparison of Systems for ΔV Required to Change Orbital Inclination

Even beyond military applications, it is advantageous to land the craft at any time, which allows for more logistical flexibility and increased frequency. In the civilian market, the logistical flexibility allowed by a reusable spacecraft with high cross-range capability will drastically reduce launch cost per pound. This is because existing infrastructure can be used multiple times to support increased flight frequency, driving down the cost of Low-Earth Orbit (LEO) transport. The cost-per-pound breakdown of operating a space vehicle as a function of flight frequency is shown below.

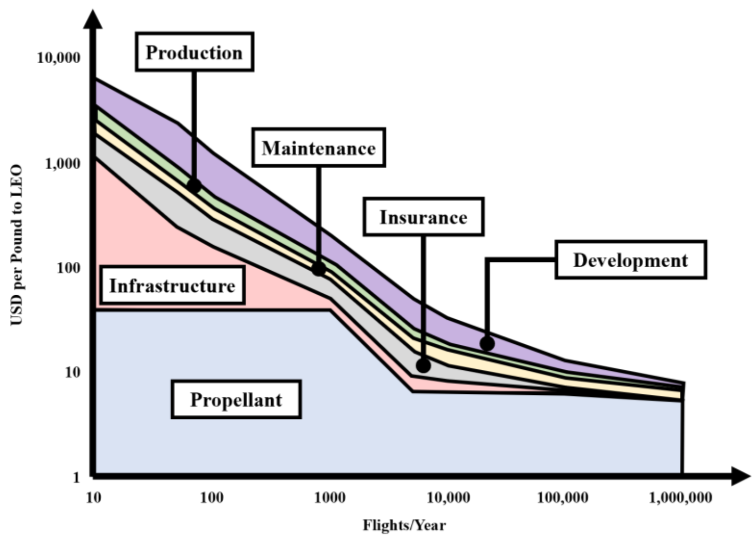

Figure 1.3: Payload Cost Per Pound vs. Flight Frequency *[7]*

A spacecraft designed to meet the critical military mission requirement can also fulfill civilian applications such as Point-to-Point (PtP) transport. This vehicle has a special economic advantage because of its reusability and rapid turn-around time. A comparison of current space-launch operations with what they could be by reducing payload costs is shown in Figure 1.4. This is an illustration of the change in human activity from an increased flight-frequency due to increasing cross-range capability [7].

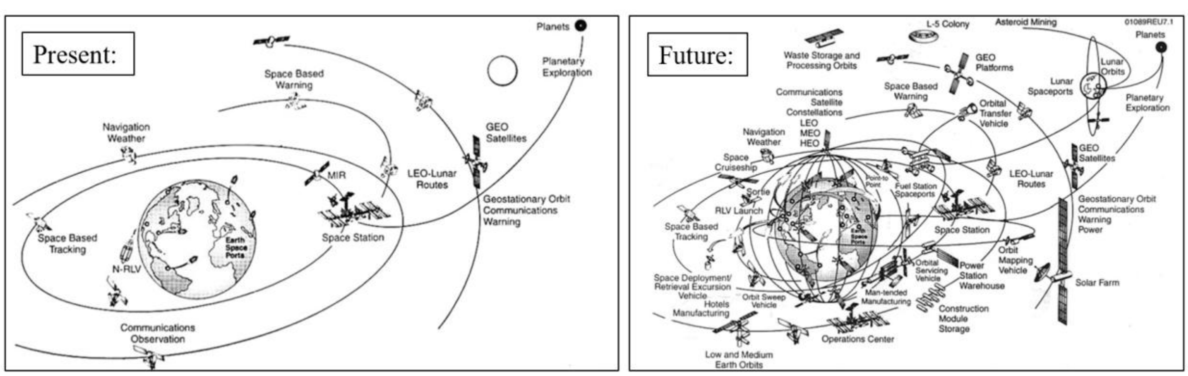

Figure 1.4: Space Activity After Lower Launch Costs from Operational Flexibility *[7]*

1.2.2 Expectations and Team Organization

The following subsections in this chapter are composed of adapted excerpts from the introductory sections of the author's senior project report [6]. They serve to provide more detail regarding the connection of ideas found in this thesis and the senior project work.

The author's senior design project is centered around reverse engineering the methodology used to develop the McDonnell Military Model 176. The focus vehicle is to be used as an example later in the thesis. This mission includes a launch vehicle and a hypersonic vehicle, and the team is responsible for validating and explaining the underlying physics behind the design to prove that it is capable of achieving mission goals. This validation method is based on extensive literature research on the topics of hypersonic flight, aerothermal heating, mission operations, stability across speed regimes, and fully-integrated sizing methodology. Trade studies are then implemented in this methodology to find further modern-day applications of this design.

There is much research which pertains to the hypersonic vehicle, such as work on the characteristics of lifting bodies and hypersonic aerodynamics. The Model 176 was recently declassified, so these documents provide a catalyst for developing the reverse engineering methodology as well as validation data. This defers from designing a completely novel vehicle, as this team's methods must now produce a physical truth that was developed historically. Design from the ground up does not have any physical validation, so there is significant room for faking erroneous results which could easily pass by review. Since there is a physical basis to verify this design, an inadequate methodology will be quickly discovered in this project's scope. However, this leaves the temptation to develop a trivial methodology which overly relies on the validation data. It must be made clear that the methodology must be derived from an independent knowledge-base of physics, multi-disciplinary analysis, and commonalities with historical vehicle precedents. The combined vehicle, with the Model 176 and launch system, is shown in Figure 1.5 alongside comparative configurations [8]:

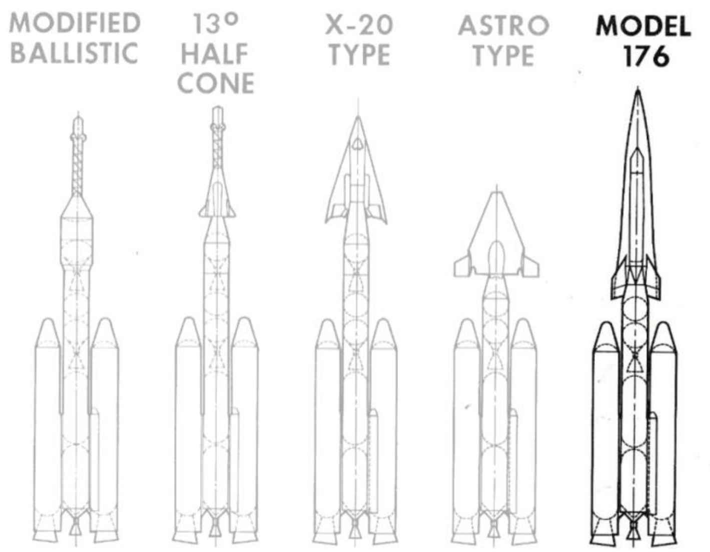

Figure 1.5: Comparative Configurations for Hypersonic Re-entry Vehicles *[8]*

For the launch platform, the existing vehicles used are SpaceX's Falcon 9 B5 and Falcon Heavy, which will be reverse-engineered. One of the main tasks of the launch team is to apply the SpaceX launching platforms (Falcon B5 and Falcon Heavy) as a new launch platform for the Model 176. One of the main advantages of these platforms is that the lowest, largest stages are fully reusable, which removes most of the expendable characteristics from the total mission.

The mission requirements for the design in question concern the development of a concept for a re-usable, manned space transport system, which is capable of orbital operations, fuel-efficient orbital maneuvering by atmospheric entry and exit, and point-to-point global transport. Such a vehicle must be integrated into some launch platform, and two sub-teams are created to divide the task of developing the upper stage hypersonic vehicle and launch vehicle.

The team is split into two main groups: one focuses on the hypersonic vehicle, the other reverse-engineers the launch system. Both teams are headed by the author, who is the chief engineer for the hypersonic vehicle. Both chiefs are involved in their respective vehicle's synthesis and are to determine costs and the business case for a mission. The structure and domains of work for the rest of the team are shown below, which is divided by discipline.

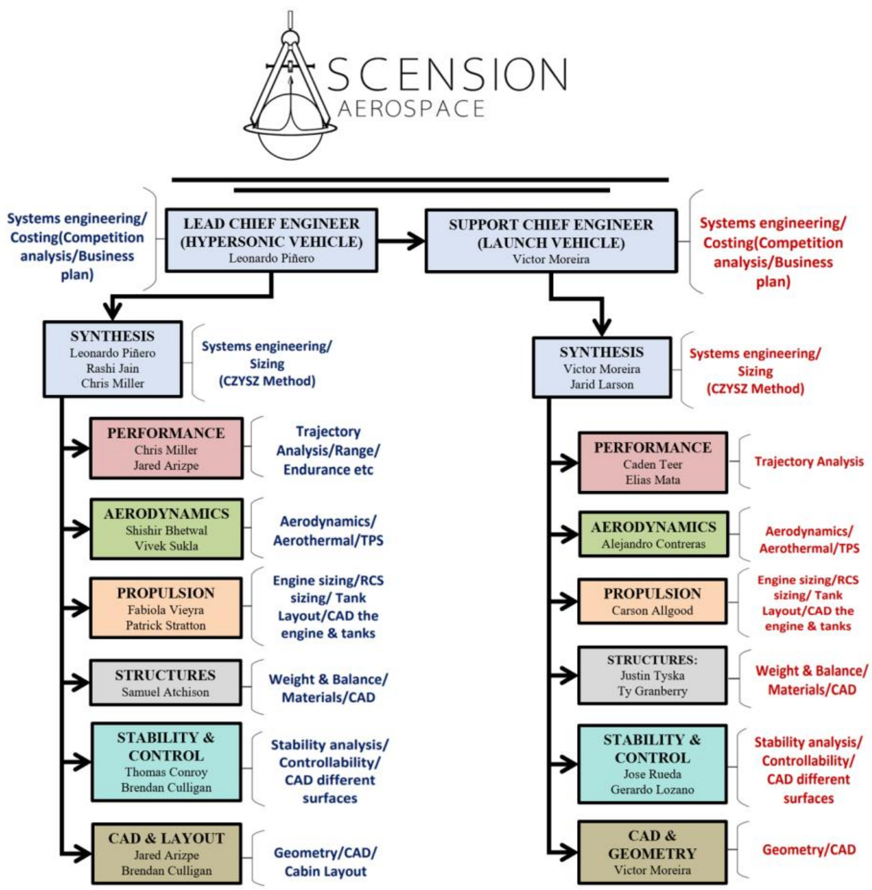

Figure 1.6: Team Structure for Senior Project *[6]*

1.2.3 Roles of Author in Team

The author's main work is to direct and bring together the many aerospace disciplines in the class team into one cohesive design. This includes writing the team report, building the methodology for multi-disciplinary analysis, creating one synthesized script, and developing a sizing methodology to provide key design parameters that meet the mission. This position is unique in that it must be familiar with the roles of all disciplines to build the bigger picture of the purpose of design.

The author must also develop a business case for the mission to meet military and market needs. The methodology and early decision-making in conceptual design usually determines the success of a program. For this reason, the role of developing the multi-disciplinary analysis and methodology bears a large responsibility.

Additionally, the role of chief engineer contains a significant human element. It is the responsibility of the author to make sure team deliverables are completed on schedule and every group member is contributing to the team effort. The chief is also the arbiter of disagreements over deliverables and domains of work. There is a general team workflow that must be nurtured, and this requires a balance between what is realistic to complete in the summer semester timeframe and what must be done to produce an exceptional project.

1.2.4 Business Case

As part of the project deliverables, the author has composed a commercial business case for a high cross-range lifting body vehicle such as the Model 176. The results here are condensed, as they only serve to provide additional context for a focus design. From this business case, a mission profile is created and its associated mission parameters are formed. These parameters connect the physical aspects of a vehicle to a commercial and military purpose.

The business case begins with the assessment of the global market for accessing low-earth orbit. After reading through several documents of market research, the author believes there is global interest in sustaining a frequent launch rate. The vehicle in question can fulfill the market need for rapid point-to-point transportation. The flight profile of such a service will include trans-Pacific and trans-Atlantic flight. The vehicle's ability to access this market is limited by launch sites, but one-way trips are still available from a launch site to a runway of suitable length.

For any transportation vehicle, the amount of the market which it can capture is a function of its range. An orbit-capable craft can capture close to the entire global market since its cross-range has global access upon reaching orbital velocity above the atmosphere. However, the orbit-capable vehicle is limited by the available launch sites. To capture as much of the market as possible, it is planned to transport passengers by conventional subsonic means to the nearest launch site before embarking across the world. By doing this, the total time of travel is expected to be within the order of magnitude of a supersonic or hypersonic flight, where all high-velocity aircraft will drastically reduce flight time for a premium when compared to conventional air travel available today.

Figure 1.7: Existing Launch Sites and Planned Launch Sites for Point-to-Point Transport

Since purchasing a ticket for high-speed flight will allow for a short flight duration (about an hour), the minimized passenger fatigue can increase productivity. Highly compensated executives likely cost their employers considerable money for their time, including during a less-productive flight. Even if the aircraft is enabled with an internet connection, the personal value an executive brings is reduced when on travel. Essentially, the company would much rather have an executive at their destination rather than in-flight. These incentives from a customer company will provide a better argument for paying for the expectedly high price per point-to-point ticket.

Realistically, due to weight sensitivity and volume constraints, the in-flight accommodations aboard an orbital point-to-point transport will be less than that of a fully-equipped first-class ticket on a larger subsonic vehicle. However, this can be more easily tolerated since the actual flight time is very short and comparable to a daily commute.

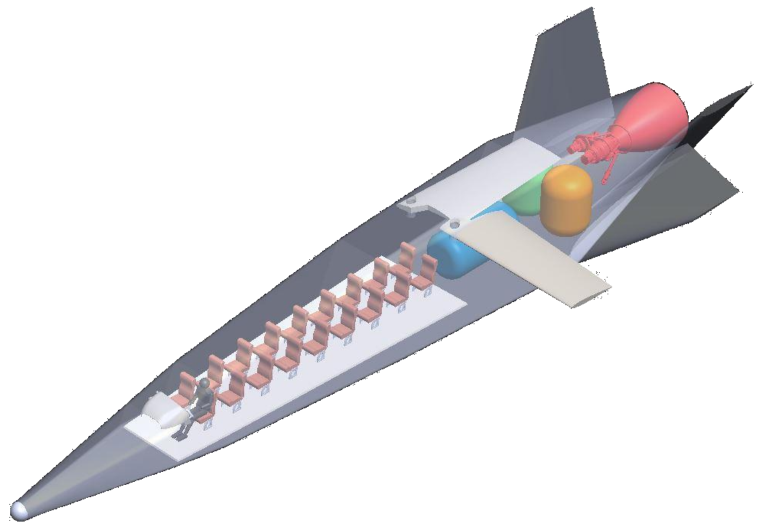

Figure 1.8: Interior Layout of Civilian Transport Variant of the Model 176 *[9]*

The market estimates for supersonic markets are conservative since orbital transport is potentially faster than a hypersonic flight (depending on the onboarding and offloading procedure). An additional conservatism is that customers are more willing to fly on a space vehicle for the cultural prestige and exhilarating experience associated with such a mode of transport. For these reasons, companies and individuals may be willing to pay a premium for tickets and the potential market for space flight is actually much larger than the market for atmospheric supersonic and hypersonic flight.

The market for paying for transport to low earth orbit is larger than the author expected and allows for enough revenue to support the program proposed by Ascension Aerospace. The tabulated values of market interest are shown below [1].

Table 1.1: US and Global Demand for Orbital Transportation [1]

Ticket Price	US Passengers/Year	World Passengers/Year	Revenue/Year ($B)
$72,000	7,500	150,000	$10.80
$24,000	137,500	550,000	$13.20
$12,000	237,500	950,000	$11.40
$6,000	600,000	2,400,000	$14.40
$2,000	1,250,000	5,000,000	$10.00

It is worth noting that these numbers are conservative given that the lack of such a service makes market estimates speculative. The source assumed that only 25% of positive respondents would actually purchase a ticket should a service for orbital transport appear. This is a conservatism and does not account for the increased demand after the presence of affordable orbital transport.

Infrastructure expenses are a function of the yearly flight rate. Fortunately, the infrastructure price per pound in orbit decreases with increasing flight rate since the relationship between flight rate and total infrastructure required is not linear. The cost of infrastructure is tabulated below [1]. Maintenance works in a similar way, with manhours per flight decreasing with increasing flight rate.

Table 1.2: Infrastructure Costs as a Function of Flight Rate [1]

Flight Rate/Year	10	50	100	1,000	5,000	10,000	100,000	1,000,000
Yearly Infrastructure Cost ($M)	300	300	350	400	400	600	1,200	3,000
Cost/Flight ($)	30,000,000	6,000,000	3,500,000	400,000	80,000	60,000	12,000	3,000

The yearly profits can now be evaluated for a 16-passenger orbit-capable transport. Using the results from previous sections, the revenues and costs of a scheduled space program are shown below.

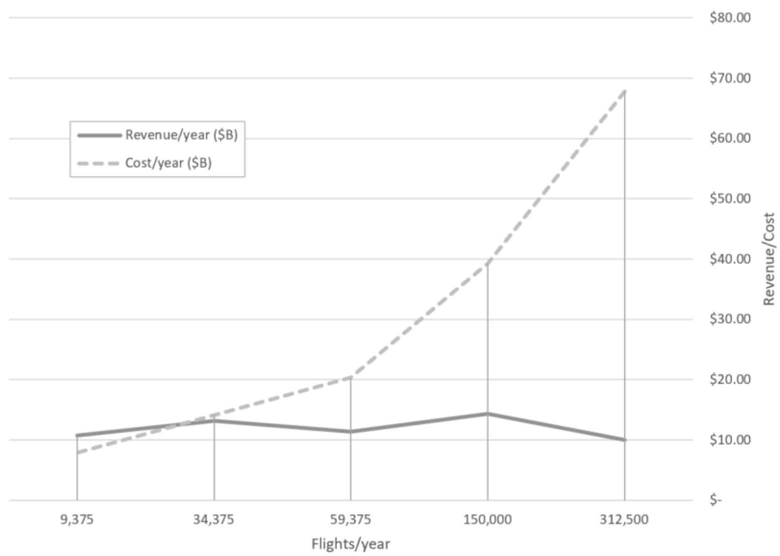

Figure 1.9: Revenues and Costs as a Function of Flight Rate

The business model is not profitable for higher launch rates since the total revenue does not match the increased costs of running such a large operation. While the price per payload pound to LEO is cheaper for such high flight rates, the global market is not large enough to pay for it. As previously mentioned, if the flight rate were decreased by increasing the ticket price, there comes a point where the demand is too low for regularly scheduled flights, which would not utilize the vehicle's high turn-rate capability.

The selected flight rate is chosen to be 8,760 per year since this corresponds to one flight per hour year-round. This is also close to the lower limit of regularly schedules flight rates for a vehicle of this size. The price per ticket can be determined as an extrapolation of the market data and is found to be 73,200 USD. By extrapolating the demand curve, the decrease number of flights allows the operation to slightly increase the ticket price. This is helpful since a decreased flight rate also increases the price per flight, as shown in previous sections.

The effects of cross-range capability on orbital wait time are shown in Figure 1.10. For a given inclination, the runway must be perfectly aligned with the orbital path if there is low cross-range capability. A reduction in wait time greatly reduces operational costs. If a vehicle could be readily sent to orbit and rapidly recovered, the relative logistical and business benefits to run such an operation are significant. This is further explored in the business case developed for the Model 176 in the senior project [6], summarized later in this chapter.

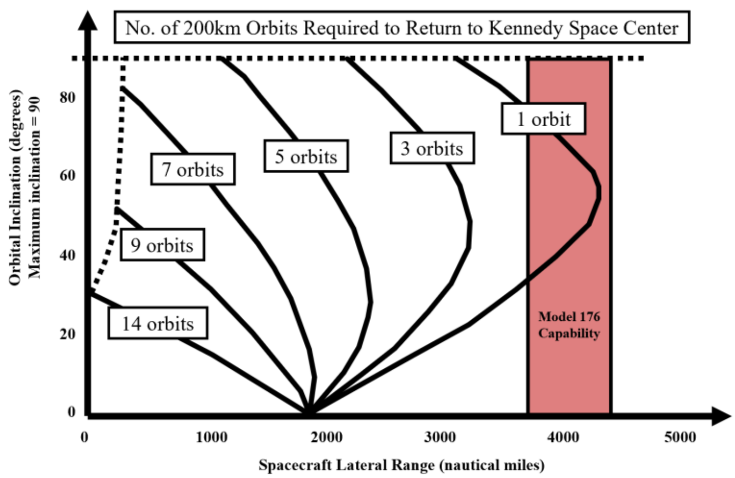

Figure 1.10: Lateral Range Capability and Inclination's Effects on Orbital Wait Time *[7]*

The size of the fleet is dependent on the expected turn-around time. If the turn-around time for these vehicles were once a day (which is the optimistic limit), then a fleet of 25 vehicles can be maintain operations. At the conservative estimated turn-around time of 48 hours, a fleet of 50 vehicles is required to meet market demand. The extra vehicles are to allow slack for maintenance and emergencies. It is quite possible that the initial flight rate is not attainable due to constant learning and troubleshooting at the early stages of operation.

The fleet will also include military variants paid for by the Department of Defense, but this cannot be predicted or scheduled in the same way as market demands. The monetary value of these contracts will need to be assessed separately. However, the civilian supported infrastructure will allow for a lower operational cost for these special vehicles.

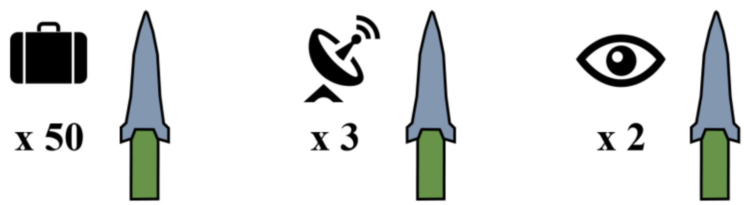

Figure 1.11: Expected Fleet Size (Left to Right): Civilian PtP, C&C, and Reconnaissance

1.2.5 Model 176 Mission Profile

The mission profile is now determined based on the operational goals for each of the three variants. The point-to-point variant will be the most common layout, as it will support the civilian market. The layout, as shown in the previous section, includes 16 passenger seats. This variant is the lightest of the three, and rightly so, as these missions will generate the least revenue in lower ticket prices to capture as much of the market as possible.

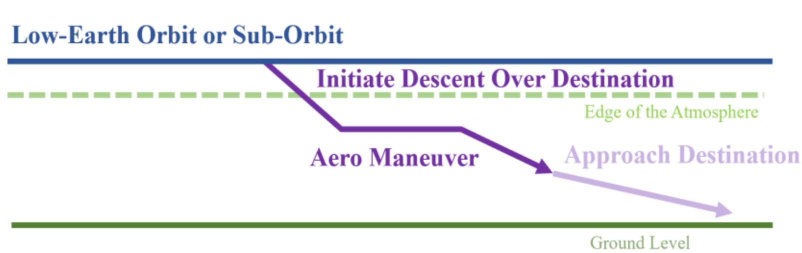

Figure 1.12: Point-to-Point Variant Upper Stage Mission Diagram

During descent, the vehicle may initiate an aerodynamic maneuver to increase its lateral ground-track. Doing this will allow the craft access to more airports outside of its direct orbital path. Much of the purpose of the point-to-point mission was described in the business case, where the main idea is to have as much access to as many destinations as possible to create the demand to support a sustained flight rate, lowering costs. These lowered costs allow for greater flight rate, and so on and so forth.

Additionally, the sustained flight rate is made cheaper by reducing the number of vehicles in the fleet. Keeping the fleet size at 50 (as described in the business case) requires a turn-around time. The Model 176 has a lateral range capability which allows for a turn-around time within the orbit. This is required if the vehicle will be ready the next day.

The Command-and-Control variant is an orbit-capable craft designed to conduct military operations independently in space. This can include satellite repair, bringing supplies and equipment to orbit, or coordinating space activities with human presence in low-Earth orbit. Whatever the operation may be, this variant is designed with a higher payload capability for life-support to sustain up to 5 astronauts. Additionally, the craft retains the capability to land safely on continental U.S. soil at any time.

A simplified diagram of the mission profile is shown in Figure 1.13. If the fact that this variant is designed for a week of operation with extra payload is ignored, this is profile is similar to the other two minus their respective added capabilities.

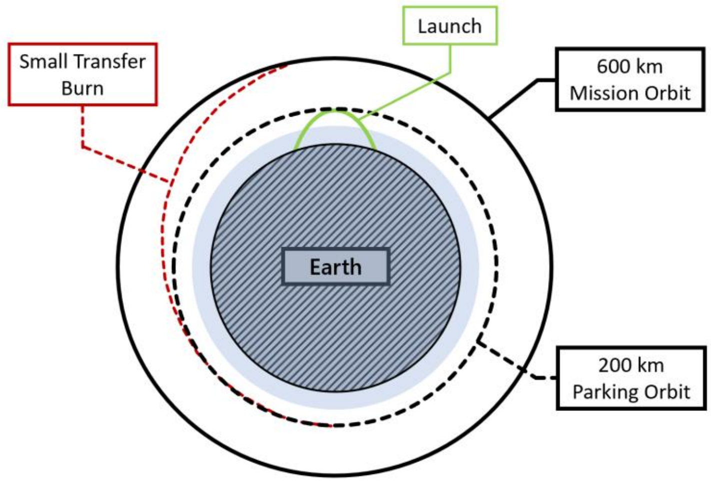

Figure 1.13: Command-and-Control Variant Mission Profile

The design-critical mission takes advantage of the lifting qualities of a hypersonic lifting body in another way. The orbiting stage can use its engine to descend into the atmosphere and make a turn by using the lift to perturb the orbit so that it can change inclination. The new orbit allows for surprise reconnaissance of any location on earth while using minimal fuel for a trajectory change. The only fuel required is used to decelerate to descend into the upper atmosphere and then to increase speed back to orbital velocity. This maneuver will be examined in depth later in the thesis. Minor orbital maneuvering can be used to alter inclination slightly or rendezvous with another body in Low-earth Orbit.

By adding this maneuver, the reconnaissance variant experiences the design-critical mission profile which is most demanding on the vehicle sizing in terms of fuel and volume required. The mission profile for the upper stage can be summarized by Figure 1.14.

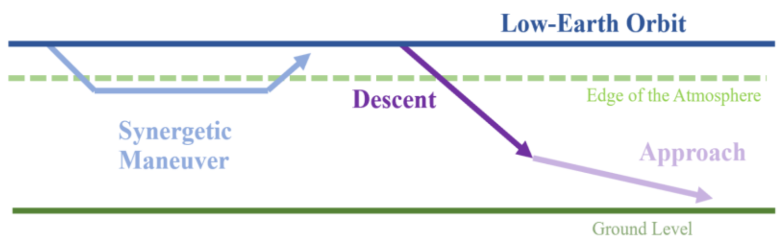

Figure 1.14: Reconnaissance Variant Upper Stage Mission Profile

The combination of this upper stage with the launch system provides the full mission profile. There is a delta V requirement at launch to insert itself into orbit, as the historical Titan III launch system was not able to carry the upper stage. This is the heaviest variant, since it needs to carry fuel for the burns shown in Figure 1.14.

The three variants are designed to operate in conjunction with each other, utilizing the same infrastructure and scheduled with respect to predictable operations to meet the existing civilian and military demands.

CHAPTER 2

LITERATURE REVIEW

2.1 Historical Spacecraft

It is important to first understand historic spacecraft designs for re-entry vehicles. From here, known design parameters can be used to validate the optimal results. This is under the assumption that the design processes used lead the programs of these successful vehicles to a near-optimal design, at least relative to a random combination of independent design parameters which would certainly fail to produce desirable results for re-entry.

2.1.1 Capsule Vehicles

The first studies on re-entry were borne out of a military objective to deliver nuclear warheads in a sub-orbital flight [10]. The warheads would be propelled into space by an inter-continental ballistic missile (ICBM) and return to Earth over an enemy target at hypersonic velocity. It was discovered that the ballistic coefficient was an important property in re-entry. This was determined by these return vehicle parameters:

$$C_{ballistic} = \frac{mg_0}{C_D A}$$

To increase accuracy and warhead velocity, a higher ballistic coefficient was needed. This makes sense, as increasing weight while lowering the drag coefficient and frontal area would allow a payload entering from orbit to retain its kinetic energy for longer portions of the entry path, since its path is more resistant to atmospheric disturbance. This was a good property for missiles, where shorter flight times and pin-point accuracy was needed for effective strikes. However, since the warhead would only slow down at lower portions of the atmosphere where the air was of sufficient density, the g-loading on the craft was not tolerable for human flight. Additionally, the warheads endured a large heat pulse, which was combatted by large metal heat sinks [10]. Materials which vaporize upon heating (known as ablative material) also protect the warhead from excessive temperatures upon re-entry.

For human passengers, the flight path angle is drastically reduced to limit the g-loading to tolerable levels of about 8g (assuming the crew is facing backwards with respect to the direction of flight [10]). The decreased entry angle and ballistic coefficients increased the flight time, so a thicker layer of ablative material was required.

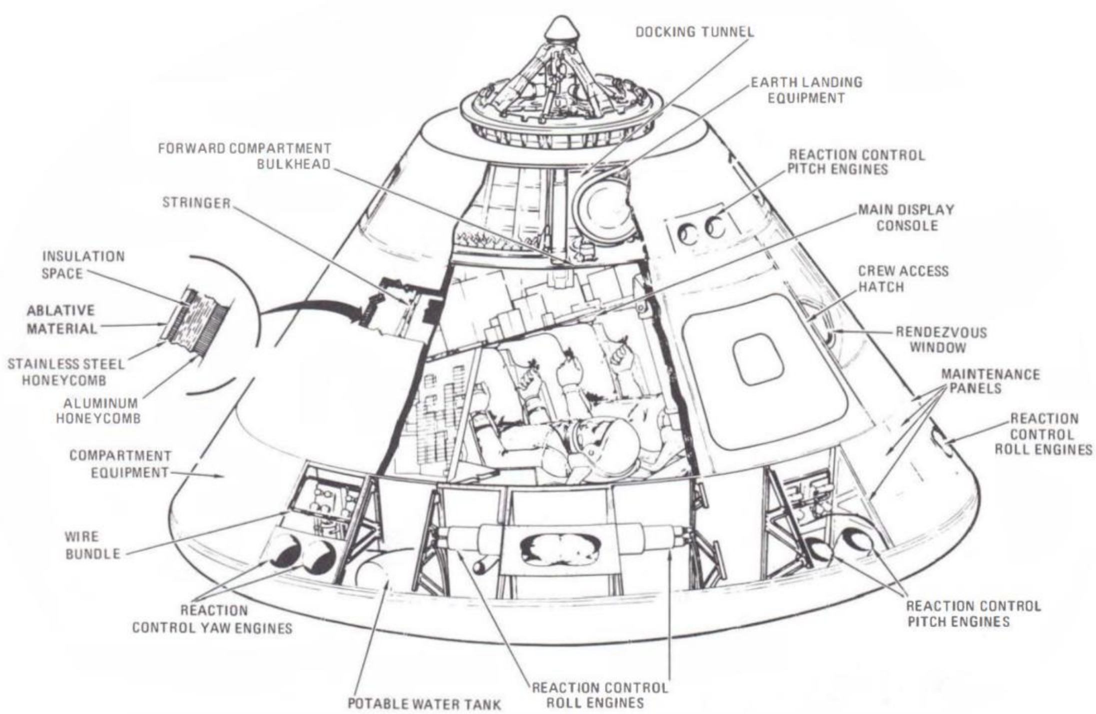

Figure 2.1: Diagram of Apollo Re-entry Capsule (doubles as Command Module) *[11]*

Capsule vehicles need a device to decelerate them sufficiently for touchdown, such as a parachute or deployable wing (i.e. a Rogallo wing). Once the vehicle was in the subsonic flight regime, the flight phase using the deployment of such a device became known as the “Decoupled Mode” [10]. This decoupled mode is a portion of the re-entry vehicle’s total mass, typically constituting about 8% of the dry weight [12].

The entry of a purely symmetric capsule is known as a ballistic re-entry, where the only significant aerodynamic force present opposite of and aligned with the direction of flight (aerodynamic drag), such as a bullet, arrow, or stone. Since there is negligible lifting force, the lift-to-drag ratio of a ballistic vehicle is near zero. The Mercury program was the only manned American program whose mission profiles used a purely ballistic re-entry capsule [10].

Capsules later developed a limited lifting capability (termed semi-ballistic), which could drastically reduce acceleration and thermal loading while increasing accuracy. Increased accuracy significantly reduced recovery costs. Lift modulation during descent also reduces thermal and acceleration loads on the craft [13].

2.1.2 Wing-Body Vehicles

Wing-body vehicles were developed as advanced aircraft with radically increased flight envelopes [10]. The concept was first introduced by Eugen Sänger, who imagined spaceflight as a manned endeavor from rocket-powered “stratospheric” aircraft. His idea was to modify existing missile designs by attaching wings and control surfaces, where by early 1944, he was working with rocket scientists for a long-range rocket plane (winged-body vehicle) to aid in the German war effort [14]. The Silber Vogel, as it was called, was to be a bomber capable of taking off from Germany and bombing the United States.

The configuration of the aircraft allowed for fuel and engines to be contained in a slender body, while wings would serve solely as aerodynamic means to control flight and the maintain lift needed for its unique flight profile.

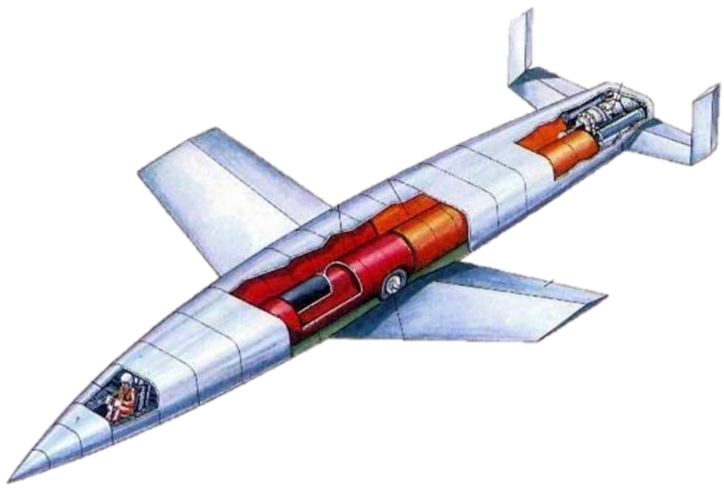

Figure 2.2 The Silber Vogel as Imagined in the Amerika Bomber Program *[15]*

The aircraft would be launched into the upper atmosphere and edge of space, and upon falling back steeply into the denser atmosphere, initiate a pull-up maneuver and “skip” back into the less dense atmosphere. Since the rocket is maintaining its velocity from the rocket launch and flight path through the upper atmosphere, significant range can be maintained, only slowly dissipating throughout the long-range flight. The intention was for the aircraft to land at least as far as the Empire of Japan. Dynamic soaring (as this skipping is called) significantly increases the range of a suborbital flight by skipping across the surface of the atmosphere as a rock would across a water pond.

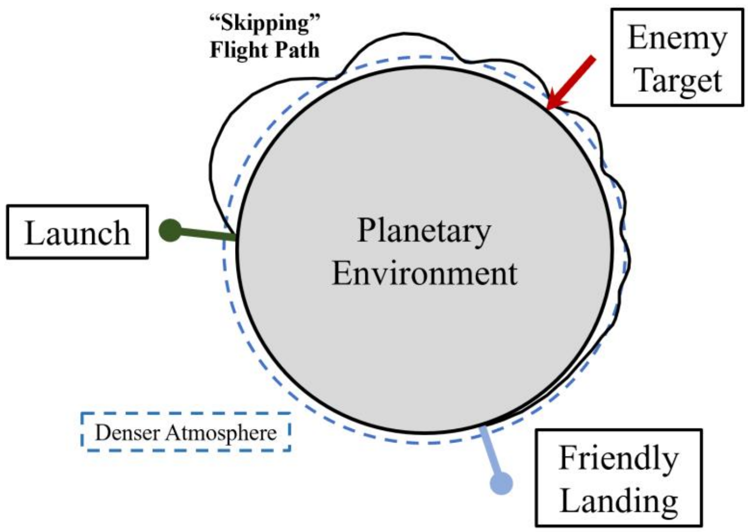

Figure 2.3: Generalized Mission Profile of the Silber Vogel (Dynamic Soaring)

The Dyna Soar was named after this flight profile, although it was only meant to maintain a long, controlled glide [10].

2.1.3 Lifting-Body Vehicles

Using a blended body vehicle requires a more complex integration of different disciplines. Since the author was reverse engineering a lifting body vehicle (blended-body shape), the development of a multi-disciplinary methodology was one of the main themes of the senior project. Something which has proven useful is the vast amount of data available from flight tests during the development of various lifting body concepts. One of the challenges of this thesis is to combine the important design parameters with those of the vehicle types in the previous two subsections. The M1-L half-cone is actually a good intermediary between ballistic capsules and blended-body flight vehicles. The lenticular shaped aircraft was a lifting body but was supposed to re-enter conventionally (as a capsule) in the upper atmosphere where the heating and deceleration was most significant [16].

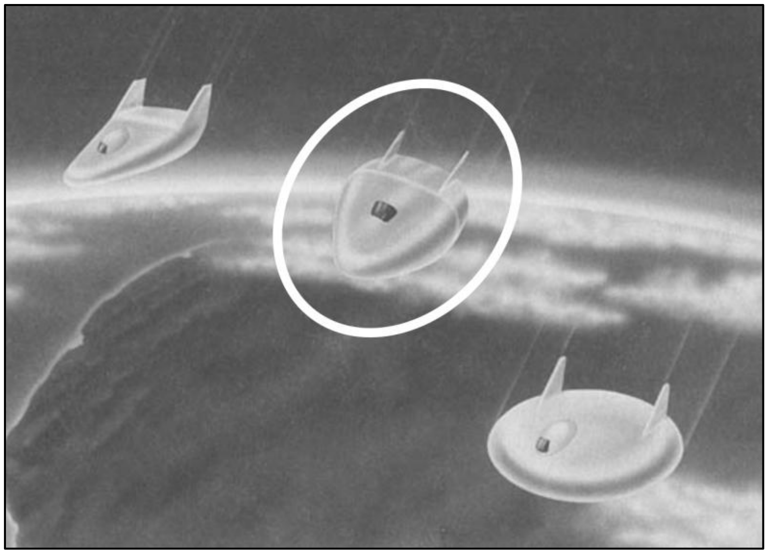

Figure 2.4: Different Types of Lifting Body Vehicles (M1-L circled) *[16]*

By viewing the historical evolution of blended bodies, an observer can see how certain design parameters evolve, such as slenderness. There is also the presence of control surfaces to maintain stability during subsonic and supersonic flight regimes to safely land as a conventional aircraft on a runway. This can be seen as a discontinuity in design philosophy: that is, capsules do not differ in shape gradually since they have reached aerodynamic characteristics to the point where they require parachutes to land safely. Similarly, lifting body aircraft such as the Hyper III require deployable wings for maintaining a high lift-to-drag ratio in the subsonic speed regime.

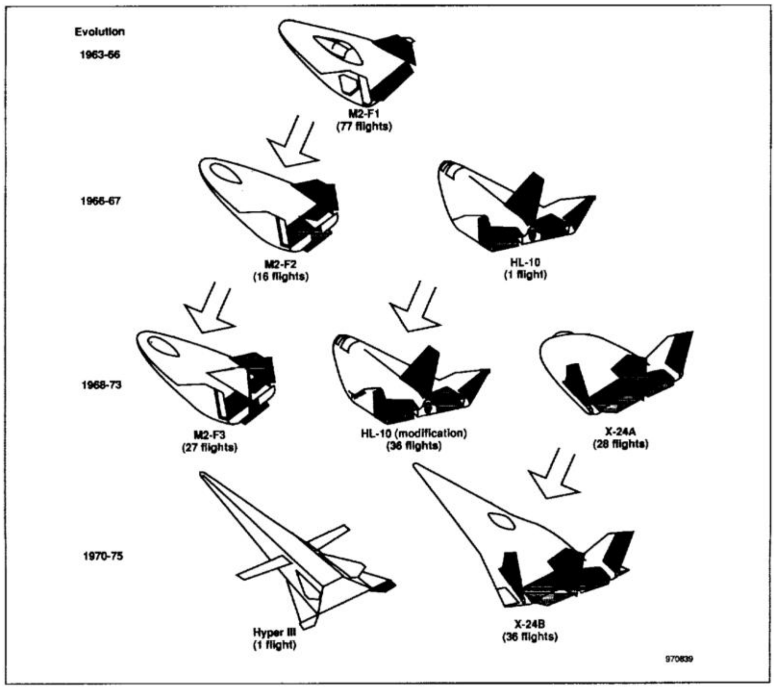

Figure 2.5: Evolution of Lifting Body Vehicles *[16]*

The changes between the X-24A and the X-24B can be seen in the drawings below. To save on costs, the frame of the X-24A was used and wrapped in the new "race-horse" shape. This shape allows for higher lift-to-drag ratios in the hypersonic speed regime [16].

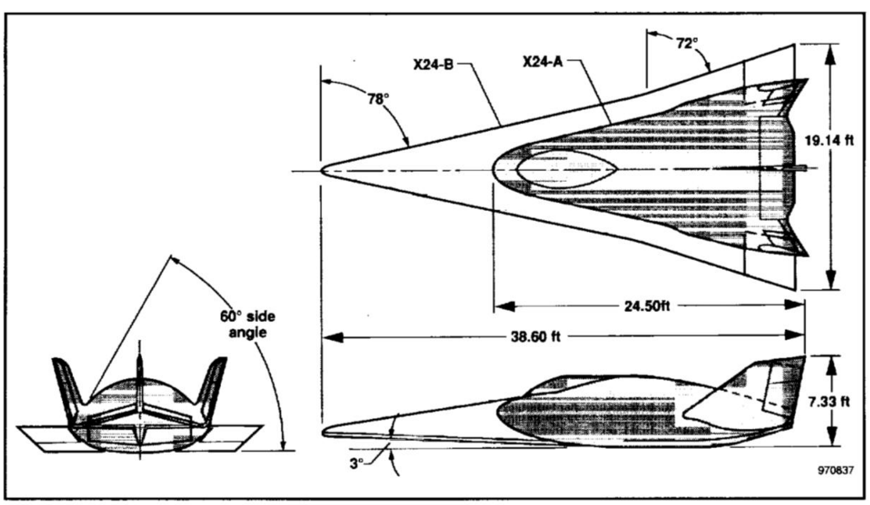

Figure 2.6: Wrapping the X-24B Geometry around the X-24A *[16]*

As thoroughly described in Chapter 1, the Model 176 is the focus of the senior project and the prime example of a blended lifting body.

2.2 Background Material for Implemented Methods

2.2.1 Vehicle Environment

When explaining the underlying physics behind this thesis, it is useful to first describe the properties of the environment in which the descent phase will take place and its initial assumptions. Returning from orbit requires the vehicle to begin at a state where it travelling very fast (orbital velocity) in a vacuum to approaching a runway near sea-level at subsonic velocity. The energy dissipation and accelerations required drive the design parameters for this stage.

The three initial environmental assumptions for trajectory analysis are as follows [3]:

i. Planets are perfect spheres
ii. Atmosphere density varies exponentially with altitude
iii. Surface velocity due to planetary rotation is negligible compared to vehicle velocity

These are reasonable assumptions for the nearby rocky planets with atmospheres: Earth, Venus, and Mars. The atmospheres of these planets can be described by an exponentially thinning gas with increasing altitude held together by the planet’s gravity. Ideal gas relationships keep the gasses afloat, and the density function based on altitude can be described by a constant planetary value known as the atmospheric scale height:

$$\beta = \frac{\bar{M} g}{R \bar{T}}$$

The atmospheric scale height can describe the density at altitude by the equation [3]:

$$\rho = \rho_0 e^{-\beta y}$$

The value of ρ_0 is not the atmospheric density at sea level, but the logarithmic extrapolation from the atmospheric scale height to sea level. This density has a value of 1.3915 kg/m^3, and the inverse of the atmospheric scale height is 7.165 km [3]. This scale height is considered to be valid for altitudes between 12 km and 100 km [2].

An important planetary value known as the gravitation constant defines the tangential velocity required to perfectly follow the curvature of a planetary body. This is dependent on the surface radius and surface gravity. The values for the gravitation constant of other bodies are shown in the table below:

Table 2.1: Physical Data of Planets of Interest and Moon [2]

Planet	*Radius [km]*	*Mass [⊕]*	*Gravitational Constant [m^3/s^2]*
Earth	6371	1.00	3.981 e14
Moon	1737	0.0123	4.890 e12
Mars	3397	0.1080	4.290 e13
Venus	6052	0.8140	3.242 e14
Jupiter	71,492	318.40	1.265 e17

Returning from a low-Earth orbit is associated with returning from a certain speed and altitude. The altitude of return is defined at the Kármán line, or 100 km above sea level [17]. The orbital velocity will dependent on the angle of entry and apogee altitude, but is known to be equal to or greater than orbital velocity, which is calculated at the Kármán line as:

$$(V_C)_{\oplus} = \sqrt{\frac{K_{\oplus}}{r}} = \sqrt{\frac{g_0 R_{\oplus}^2}{100\ km}} = 7.84\,\frac{km}{s}$$

The factors used above will define the significant centrifugal contribution keeping the vehicle in steady flight.

2.2.2 Vehicle Flight Path and Loads

The region of interest in the atmosphere described in the previous section is a roughly 20 km band where the density increases by a factor of about 20 [3]. It is in this region where peak heating and acceleration is experienced by the vehicle. Chapman's analytical method [3] for studying vehicle entry applies to these regions where the vehicle is kept flying due to a combination of orbital centrifugal forces and aerodynamic lift. When the flight path angle matches that which is predicted by conventional flat-earth subsonic flight (solely a function of lift-to-drag), the spacecraft is now low enough in the atmosphere to perform as an aircraft would and is outside the domain of the re-entry analysis. Likewise, outside of the atmosphere, the flight path angle can be predicted by orbital mechanics and is not relevant to the flight phase examined. Figure 2.7 shows the region analyzed as a solid line [3]:

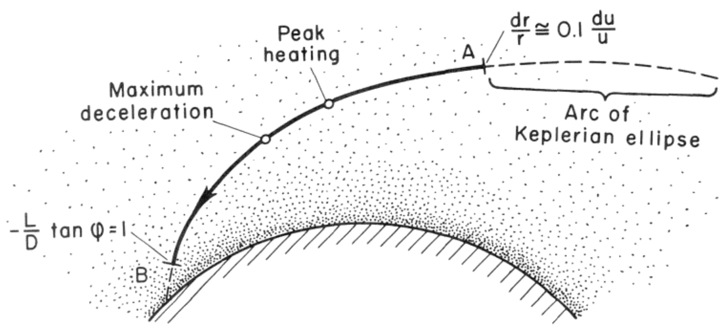

Figure 2.7: Region of Flight where Chapman's Analysis is Significant *[3]*

In summary, the motion of the vehicle can be described by a dimensionless variable as a function of spacecraft velocity and constant parameters [3]:

$$Z \equiv \left[\frac{\bar{\rho}_0}{2\left(\frac{m}{C_D A}\right)}\sqrt{\frac{r}{\beta}}\right]\bar{u}e^{-\beta y}$$

For the purposes of design, it is important to note that the driving design parameters of this function are the drag coefficient and reference area. These will be tweaked according to how they affect this function of normalized velocity $\bar{u}$. The differential equation describing the vehicles path is explained below [3]:

$$\bar{u}Z'' - \left(Z' - \frac{Z}{\bar{u}}\right) = \frac{1-\bar{u}^2}{\bar{u}Z}\cos^4\gamma - \sqrt{\beta r}\left(\frac{L}{D}\right)\cos^3\gamma$$

The left side of the equation describes the vertical acceleration and the vertical drag force. The right side's first term describes the difference between the gravity and centrifugal force, and the last term describes the lift force. In this location, the lift-to-drag ratio may be modulated to control the flight path. This equation is useful since it allows extrapolation of previous data on Earth to other atmospheres and mission profiles. The solutions for Z change based on the type of vehicle analyzed, since certain terms can be disregarded. The applied solutions are tabulated Table IV [3]:

Table 2.2: Solutions for Z Based on Vehicle Type [3]

Solution	*Vehicle*	*Dropped Term and Assumptions*
$Z_I = \sqrt{\beta r}(\sin\bar{\gamma})\bar{u}\ln\left(\frac{\bar{u}}{\bar{u}_i}\right)$	Ballistic	Gravity, Centrifugal and Lift Forces
$Z_{II} = \frac{1-\bar{u}^2}{\bar{u}\sqrt{\beta r}\left(\frac{L}{D}\right)}$	Glide	Vertical Acceleration and Vertical Drag; $\cos\gamma \cong 1$
$Z_{III} = \bar{u}\left[\frac{Z_i}{\bar{u}_i} + \left(\sqrt{\beta r}\right)\gamma_i\ln\left(\frac{\bar{u}}{\bar{u}_i}\right) - \frac{\sqrt{\beta r}}{2}\left(\frac{L}{D}\right)\ln^2\frac{\bar{u}}{\bar{u}_i}\right]$	Skip	Gravity and Centrifugal Forces; $\cos\gamma \cong 1$
$Z_{IV} = \bar{u}\sqrt{\beta r}\left[\gamma_i\ln\bar{u} - 0.5\left(\frac{L}{D}\right) - \frac{0.25}{\beta r\gamma_i}\ln^2\bar{u}\right]$	Satellite Decay	Small initial flight path angles

With this general equation, some useful values may be found, such as tangential acceleration [3]:

$$a_\theta = -\frac{du}{dt} = \frac{g\sqrt{\beta r}}{\cos\gamma}\bar{u}Z$$

While g and r are local values, for Earth they may be assumed to be the constant surface values. Additionally, while the flight path angle is small, the cosine denominator may be assumed to be unity. Applying earth values, the equation for the critical tangential acceleration is (in g's):

$$-\frac{1}{g}a_\theta \cong 29.82\bar{u}Z$$

This tangential acceleration value is critical for manned missions and must not be exceed more than 5 g's for the human crew's safety [2].

To plot the flight path on Earth, the descent angle and distance travelled can be computed:

$$\gamma = \sin^{-1}\frac{Z' - \left(\frac{Z}{\bar{u}}\right)}{\sqrt{(\beta r)_{earth}}} = \sin^{-1}\frac{Z' - \left(\frac{Z}{\bar{u}}\right)}{28.92}$$

$$\frac{\Delta s}{r} = \frac{1}{\sqrt{(\beta r)_{earth}}}\int_{\bar{u}_2}^{\bar{u}_1}\frac{\cos\gamma\, d\bar{u}}{Z} = \frac{1}{28.92}\int_{\bar{u}_2}^{\bar{u}_1}\frac{d\bar{u}}{Z}$$

It is important to keep in mind that this analysis requires Z to be nonzero and the flight path angle γ to be small, which is true for the critical regions of the descent stages of a spaceplane.

2.2.3 Vehicle Design Parameters

The goal of this thesis is to optimize a design to save weight while meeting the mission requirements for a manned spaceplane. The descent flight phase is one of the largest contributors to the total weight of a spacecraft, since any thermal protection system or design features tailored for performance at this stage must be carried all the way to the end of the mission. The added weight for this phase is therefore significant since it detracts from the available payload to space for a given launch system. Additionally, to launch a given payload and the weight of the upper-stage vehicle, the launch system must be exponentially larger to meet a mission trajectory according to the rocket equation [2]:

$$W_{launch} = W_{empty} e^{\frac{\Delta V_{req}}{I_{sp} g_0}} = (W_{(descent\ vehicle)} + W_{payload}) e^{\frac{\Delta V_{req}}{I_{sp} g_0}}$$

One performance guideline for manned spacecraft is the deceleration limitation. This is dependent on the weight of the spacecraft, flight path angle, and drag properties. The equation for acceleration during descent, where $\sin(-\gamma)$ is negative [2]:

$$a = \left(\frac{-W \sin\gamma - D}{W}\right) g$$

For this reason, the vehicle weight required to support a given returning payload is a key parameter in determining the cost effectiveness of a descent vehicle. The structural weight is correlated to the volume of a capsule and planform area of a glider. The volume required can be determined by the following mission parameters [12]:

$$VOL_{crew}\ [m^3] = 1.247 N_{crew}^{0.136} N_{days}^{0.150}$$

CHAPTER 3

METHODOLOGY

3.1 Geometry Definition

3.1.1 Parameters Chosen

With the three classes of vehicles studied in the previous chapter (capsule, wing-body, and blended-body), the geometric parameters are chosen by common attributes which can be scaled in a continuum. In this way the same aspects of two radically different vehicles can be numerically compared. Additionally, these parameters must have first-order relevance to the performance of the spacecraft. For instance, it would not make sense to include the dimensions of a crew entry hatch as these would have a negligible effect on vehicle parameters such as volume available, structural weight, or lift-to-drag ratio. It is important to state this now, as one of the largest differences between many of the representations of vehicles studied here and their real-world analogues is that their windshields disrupt a simpler design. Obviously, there was a second-order correction for pragmatic reasons, specifically pilot visibility (even if that means deviating from the conceptual aerodynamic design).

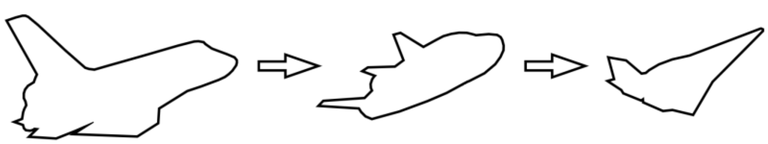

Figure 3.1: Different Historical Configurations must be able to Relate on a Continuum

The first parameter is chosen for its simplicity in fully describing a body with one radial dimension: a sphere. Already, this shape has characteristics that could be assessed in terms of re-entry performance (volume, planform area vs. surface area, structural weight, etc.). This simple configuration is shown in Figure 3.2, using aircraft coordinates along with first-order variables to be used in defining vehicle performance.

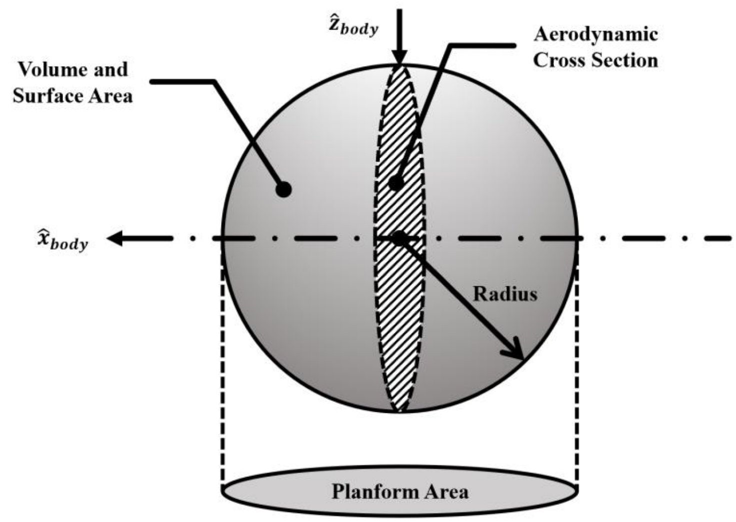

Figure 3.2: Spherical Spacecraft Design as a Re-entry Aircraft

The sphere, however, is not used because it is not an advantageous configuration given the physics of aerodynamic flight. However, if one sufficiently alters the environment or mission, the sphere can quickly become more attractive. This is exemplified in the Apollo program, where the shape of the lunar lander ascent stage was never designed to interact with the atmosphere, so structural weight became the largest concern and a spherical shape was chosen. If we were to create an environmental continuum between that of Earth sea-level atmosphere and a vacuum (described by density and atmospheric scale height), one could also assess the performance of different shapes according to some parameter which increases slenderness.

This parameter is the chord length of what used to be a sphere (which only had a radial parameter). This new parameter duplicates the sphere and specifies the distances between the two bodies. The entire geometry is still closed by a geometric loft, as shown in Figure 3.3. An important aspect of this choice is that a single sphere (as shown in Figure 3.2) can still be created by setting the chord length to approach zero. These two parameters defined by these rules can build pill shapes and can already approximate the fuselage of atmospheric aircraft.

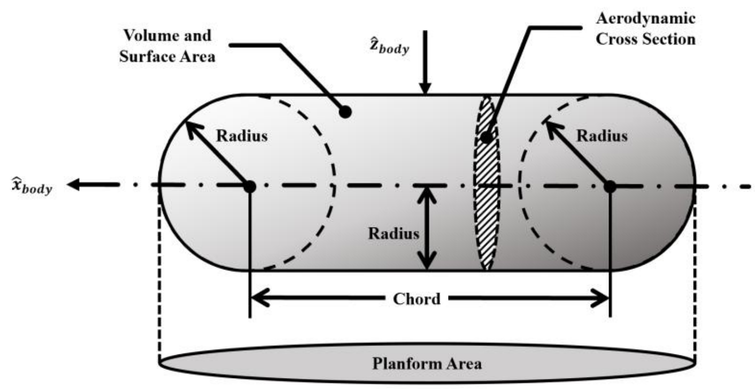

Figure 3.3: New Generalized Design Now defined by Chord and Radius

It is evident that the most common aspect of all space vehicles is that they have a body which could store fuel, propulsion, and payload required to complete a mission. The overall shape chosen is a rounded cross section, which can approximate other polygonal cross sections such as a diamond or trapezoid. The selection of a rounded cross-section also accurately represents fuselage bodies and axially symmetric capsules.

Two more parameters are added to allow for design flexibility. The first added parameter is simply adding a degree of freedom to the pill design: the radii of the pill-shape can now have different values. By doing this, conical shapes can be approximated, and the nose radius can be decreased while allowing a large aft radius for storing fuel and a propulsion system in the aft region.

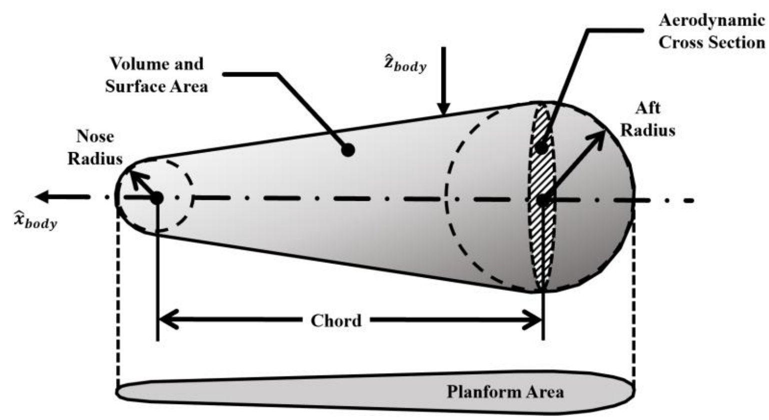

Figure 3.4: Generalized Design after Unlocking the Equal Radii Constraint

At this point, some new rules are given to this general design. The aft radius will now only be used to describe the aft cross section, which makes this dimension constrained to the y-z plane in the aircraft body coordinates. This is due to the impracticality of a rounded or domed aft section configuration, as this area is usually flat to be a flush mate with lower stages, reducing the structural weight of the combined vehicle. This is actually one of the disadvantages of using an ovoid shape for a re-entry capsule, as a truss system must be added to the combined vehicle for proper interface with lower stages [12]. This truss system will most likely require aerodynamic fairings to endure the atmospheric loads during launch. Additionally, this staging interface can be reserved for an area to place the nozzle of the propulsion system.

The second parameter added is the span, converting the axially-symmetric cross-section to an elliptical one. This further constrains the aft radial parameter to one dimension along the z-axis and the nose radius to the x-z plane. By doing this, the cross section can be changed to more accurately describe blended body vehicles. As will be later discussed, increasing the span increases the planform area and the surface area. These new geometric conditions finalize the body section of this generalized design.

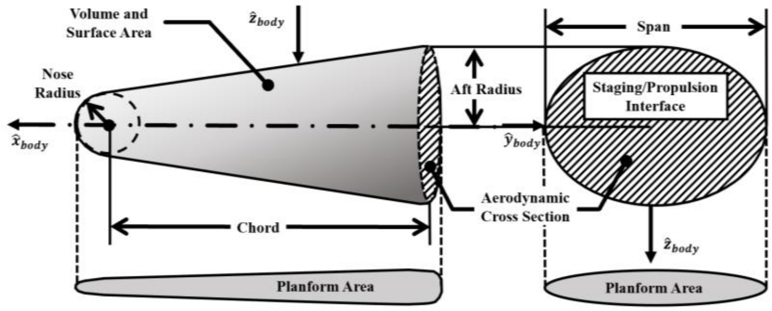

Figure 3.5: General Design Described by Nose and Aft Radii, Chord, and Span

It is important to re-iterate that these four parameters can be made into special cases such as the pill shape or sphere by setting the span to equal the radii, set the radii equal to each other, and possible setting the chord to zero (if a sphere is desired). The main idea is that the original, simple geometry is not lost, but flexibility and applicability is increased by adding these four important parameters.

3.1.2 Superimposed Wing

The body of the spacecraft is now constructed, and this alone can describe many re-entry vehicles, such as capsules or lifting bodies. Again, since there are only four geometric parameters, second-order characteristics such as windshields or multiple sweeps cannot be described. However, first-order trends can be identified along parameter axes for these vehicles. This theme continues by adding a second element to capture a major configuration feature of historical re-entry vehicles: the wing. Vehicles such as the Dyna Soar or the X-37 cannot be described only defining a fuselage, so the option to superimpose a wing body must now be included.

The existing fuselage is now rotated to be facing the x-y plane, demonstrating the planform area of the vehicle. The key parameter affected by adding a wing is the planform area with a negligible increase in volume. The increased surface area with minimal wing volume creates a radically increased structural weight, which must include thermal protection. Minimal wing volume also does not allow the storage of fuel or payload. This is the cost of increasing the planform area.

The wing is defined by two new geometric parameters: the wing's root chord and the wing span. The end-points of these dimensions create a delta-shape, which is the simplest to define and characteristic of planforms in the hypersonic speed regime.

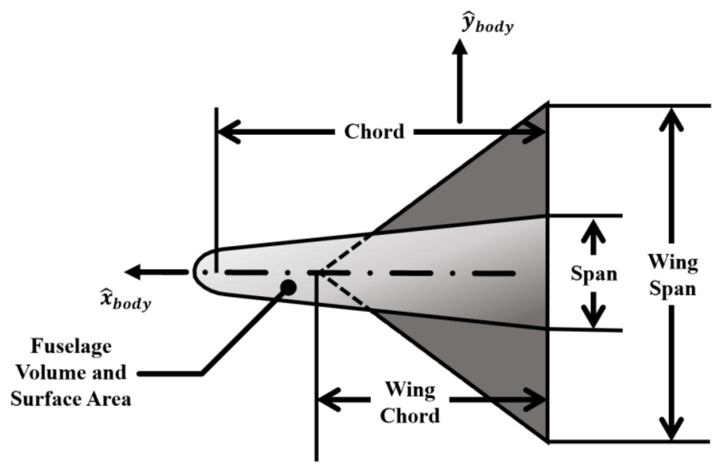

Figure 3.6: Generalized Fuselage with a Superimposed Generalized Delta Wing

The addition of a wing can be further defined by a dihedral angle for directional stability. However, to do this the x-y plane projection (planform area) is decreased without changing the overall surface area associated with zero volume (wing size). Directional stability is obtained by incurring a structural weight cost if the lifting planform area is held constant.

3.1.3 Historical Validation of Geometry

With these parameters, a first-order configuration can now be made to represent the majority of historical vehicles. The sample of historical vehicles is now shown in this section to validate the geometric definitions built in this section.

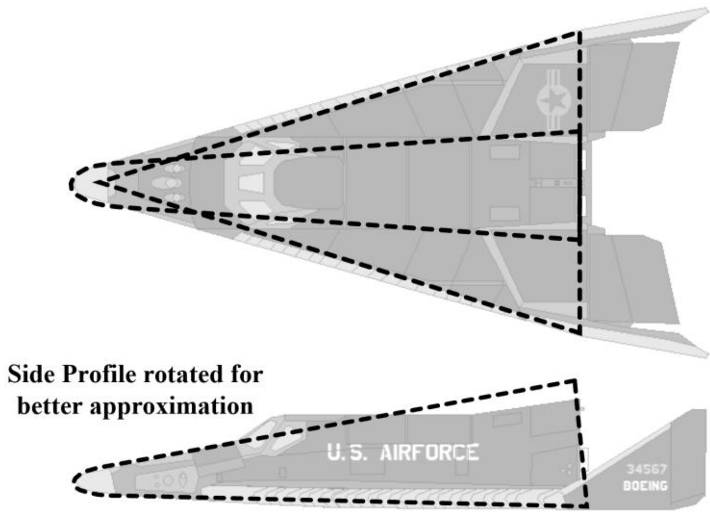

Figure 3.7: X-20 Dyna Soar Represented by Geometric Parameters *[18]*

There is some obvious error (notice the windshield), but as mentioned before, this an acceptable loss in order to build a parametric continuum between this configuration and something like a Mercury capsule, as shown in Figure 3.8.

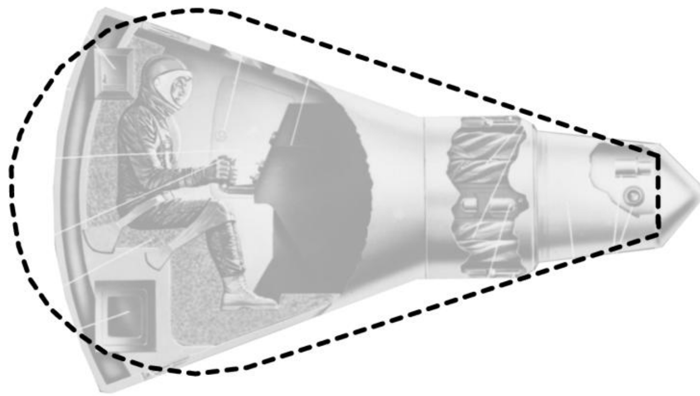

Figure 3.8: Mercury Capsule Represented by Geometric Parameters *[19]*

The nose radius is now shown to be larger than the aft radius, but it still remains the nose radius as its definition extends along the x-z plane as opposed to being constrained to the z-axis like the aft radius. It is also worth noting that unlike the X-20 Dyna Soar, the Mercury capsule is axially symmetric, so its span parameter is set to be equal to the aft radius. The parameters are set so that there is a close approximation for volume and surface area. However, to do this, the nose radius is decreased, which will over-estimate the heating loads. There are also no wings superimposed on this vehicle.

Lastly, the geometric parameters will represent the focus vehicle of the author's senior project, shown in Figure 3.9. This vehicle is a blended body with a trapezoidal cross section (approximated here as an ellipse scaled to equal cross-sectional area). Without wings, this lifting body has a high slenderness and is expected to be the highest performing vehicle.

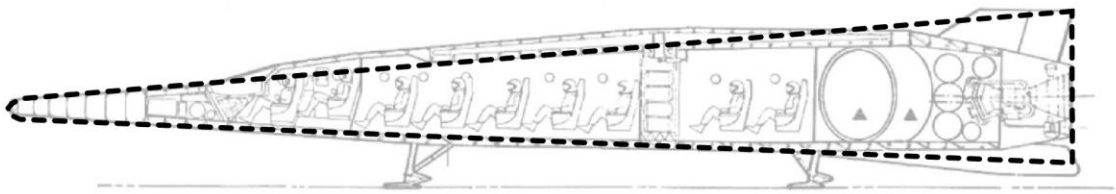

Figure 3.9: Model 176 Represented by Geometric Parameters *[8]*

It has been shown that the parameters presented can re-create a wide variety of historical spacecraft upper stages. The next stage is to take these parameters and link them to performance measures which can assess the viability of these configurations across several missions and environments.

3.2 Geometry Analysis

3.2.1 Planform Area

The fuselage planform area is easily computed as a function of the geometric parameters, which are now abbreviated as proper variables: $r_{aft}, c,\ r_{nose}, b$. The nose's contribution is first ignored and can be computed as a half-ellipse. As seen by the Mercury capsule, the nose planform area can make up a significant portion of the total planform area.

$$S_{body} = S_{loft} + S_{nose} = \left[\frac{bc}{2}\left(1 + \frac{r_{nose}}{r_{aft}}\right)\right] + \left[\frac{\pi b r_{nose}^2}{4 r_{aft}}\right]$$

If a wing is added, the shared planform area between the two bodies (wing and fuselage) is not computed to avoid double-counting. Instead, only the exposed planform area is computed.

$$S_{wing} = \frac{\frac{1}{2}\left(b_{wing} - b\right)^2}{\frac{b}{c}\left(1 - \frac{r_{nose}}{r_{aft}}\right) - \frac{b_{wing}}{c_{wing}}}$$

Sometimes, the wing geometry may be modified to a point where it is completely enveloping the body, in which case the planform area of the vehicle is equal to the planform area of the wing. Conversely, the wing may become completely obscured by the body and output a negative value by mathematical definition, in which case the planform area due to the wing is told to become a value close to zero.

3.2.2 Wetted Area

Wetted area is computed by numerically computed by taking the circumference of the ellipse and extruding it by a small step size along the x-axis. This step size is set as a small proportion of chord length. It is important to note that the numerical error increases as the sweep angle decreases, as each step along the x-axis has a 90-degree sweep. Since hypersonic vehicles typically have a high sweep angle, small-angle assumptions will hold true for each step along the x-axis.

There is no exact solution for finding the circumference of an ellipse, so this is also an approximation and surprisingly complicated [20].

$$Circ(x) \approx f\left(r(x), \frac{b(x)}{2}\right) = f(p, q)$$

$$= \pi(p+q)\left(\frac{3(p-q)^2}{(p+q)^2\left(\sqrt{-\frac{3(p-q)^2}{(p+q)^2}+4}+10\right)}+1\right)$$

Where the local variables are found as a function of geometric parameters and axial location:

$$r(x) = r_{aft} + \frac{r_{nose} - r_{aft}}{c}x$$

$$b(x) = \frac{r(x)b}{r_{aft}}$$

The staging/propulsion interface in the aft part of the vehicle is not considered for wetted area, as it is not exposed to re-entry conditions. In some special circumstance, considering this interface area as wetted area is as easy as adding the area of that ellipse.

The nose surface area is that of a half ellipsoid, which is also a complicated mathematical approximation [20].

$$S_{wet} = (S_{wet})_{loft} + (S_{wet})_{nose} = \left[\int_0^c Circ(x)Hdx\right] + 2\pi\left[\frac{1}{3}\left(2\left(\frac{r_{nose}^2 b}{r_{aft}}\right)^{1.6} + r_{nose}^{3.2}\right)\right]^{\frac{1}{1.6}}$$

Where H is user-determined as a trade-off between accuracy and computational speed. In this study, it is set to one two-hundredth of the chord length as this calculation will be made many thousands of times each time the script is run.

3.2.3 Volume

Volume is computed similarly to wetted area, where the lofted section is computed numerically along x-axis steps sized as a small proportion of the vehicle chord. Instead of local circumference, local area is computed. The formula for local elliptical cross-sectional area is simpler and exact, using the local variables $r(x)$ and $b(x)$.

$$A(x) = f\left(r(x), \frac{b(x)}{2}\right) = f(p,q) = \pi pq$$

The lofted volume is found by combining the numerically integrated lofted volume and the nose volume (half-ellipsoid). The wing does not contribute to the total vehicle volume.

$$VOL = VOL_{body} = VOL_{loft} + VOL_{nose} = \left[\int_0^c A(x)Hdx\right] + \left[\frac{2\pi r_{nose}^3 b}{3r_{aft}}\right]$$

3.2.4 Küchemann's Tau

Tau is simple to calculate, as it is a ratio function of two previously computed variables: volume and planform area. Tau is important for determining the aerodynamic characteristics of the vehicle, particularly lift-to-drag ratio. It is defined by this ratio [7].

$$\tau = \frac{VOL}{S_{plan}^{1.5}}$$

<u>3.3 Vehicle Analysis</u>

3.3.1 Structural Weight

The structural weight is considered to be linearly correlated to the wetted area according to a technology index. This index is specific to the state-of-the-art in materials science, whose value is found in literature for re-entry vehicles. It is worth noting that the smaller nose radii will disproportionately require a higher structural weight due to an increased heat flux.

$$W_{str} = I_{str} S_{wet}$$

The structural index is set to $I_{str} = 17.1 \frac{kg}{m^2}$ for re-entry vehicles [7].

3.3.2 Propulsion System

The propulsion system is included according to typical orbital maneuvering engines considered sufficient to follow the proposed re-entry and synergetic trajectories. The propulsion system is paid for by engine weight and volume, and in return will give the vehicle a property of non-zero specific impulse, depending on the type of engine "bought" by the weight and volume budget.

The payload weight and volume will now affect the remaining volume available for propellant. A vehicle with maneuvering capability must have enough volume available to contain the engine and payload. In this way, there is volume available for propellant.

$$VOL_{ppl} = VOL - VOL_{eng} - VOL_{pay}$$

Where the following condition must be met for a maneuvering vehicle:

$$VOL > VOL_{eng} + VOL_{pay}$$

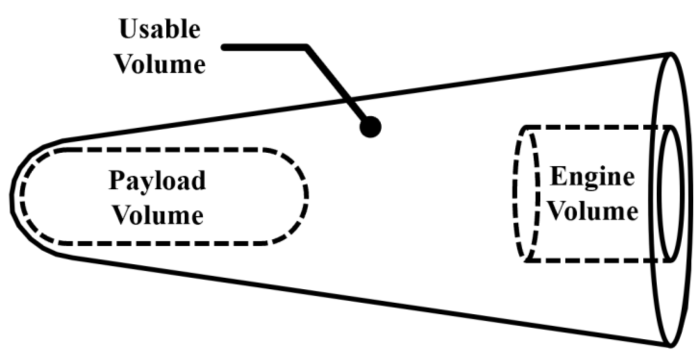

Figure 3.10: Volume Breakdown for First-Order Vehicle

The rest of the volume will be filled with propellant, where the volume of the structure is considered to be negligible for first-order analysis. The weight of the propellant is determined by the mixture ratio required by the engine.

3.3.3 Delta V

The weight of the propellant and the structural weight will determine the vehicle's mass ratio.

$$MR = \frac{W_{full}}{W_{empty}} = \frac{W_{eng} + W_{pay} + W_{str} + W_{ppl}}{W_{eng} + W_{pay} + W_{str}}$$

This mass ratio combined with the specific impulse will determine the delta V available to the spacecraft by the rocket equation.

$$\Delta V_{available} = g_{\oplus} I_{sp} \ln{(MR)}$$

3.3.4 Lift to Drag Ratio

The lift-to-drag ratio can be computed as an empirical function of tau. This is found in literature from the result of flight and wind tunnel testing of various bodies [21].

$$\frac{L}{D} = \frac{A(M+B)}{M}\left[\frac{1.0128 - 0.2797\ln\left(\frac{\tau}{0.03}\right)}{1-\frac{M^2}{673}}\right] \text{ where } A = 6 \text{ and } B = 2$$

This equation applies only to a specific range of tau, so conditional statements are created to bound the possible lift-to-drag ratios between zero (ballistic) and three (highest expected performance).

A modified estimation for lift-to-drag performance is created from data points found in reference [22]. The trend is strongly correlating to a negative linear slope as shown in Figure 3.11.

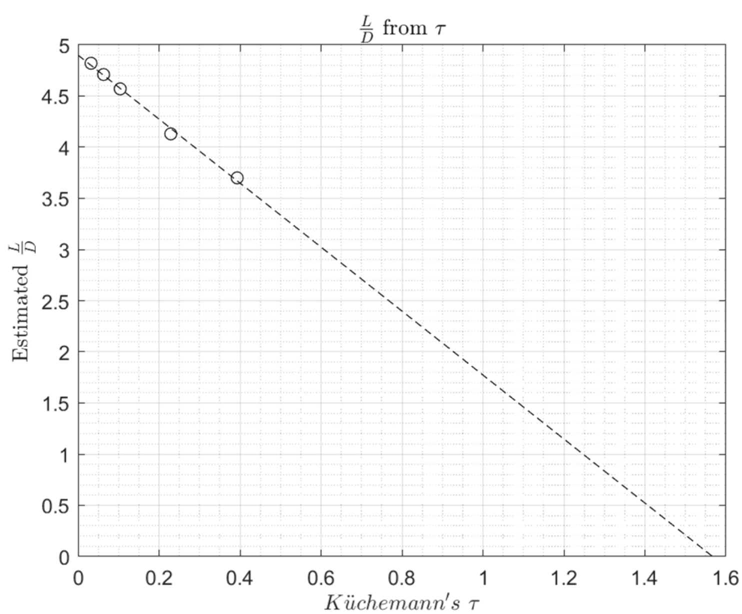

Figure 3.11: Alternative Lift-to-Drag Ratio Estimation Method from Tau

3.4 Performance Analysis

3.4.1 Payload Capability

The first assessment of performance is that of the payload capacity of the vehicle with respect to the launch weight. The full weight of this upper-stage vehicle is the payload of the lower stages. According to the rocket equation, increasing the full weight will significantly increase the weight of the launch vehicle. This will increase the total cost of carrying a given payload. The user will specify the importance (signified as A_{PI}) of payload capability depending on the anticipated budget for the launch vehicle.

$$PI_{pay} = \frac{A_{PI}W_{pay}}{W_{eng} + W_{pay} + W_{str} + W_{ppl}}$$

Vehicles which place high priority on PI_{pay} will be driven to reduce the propellant and structural weight by decreasing the geometric dimensions. Consequentially, increasing the importance of this performance index will take a toll on the other two performance indices.

3.4.2 Synergetic Maneuver

The vehicle's ability to perform a synergetic inclination change is a function of the available fuel and aerodynamic properties. This assessment is determined from Nyland's analysis of synergetic maneuvering according to $\Delta V_{available}$ and L/D.

The vehicle's capability is assumed to be at a maximum performance when the angular change of inclination reaches 90 degrees. This is due to the assumed conical angle of 45 degrees, the value of which was selected as the best compromise to minimize maneuver heating and achieve a full inclination maneuver [5].

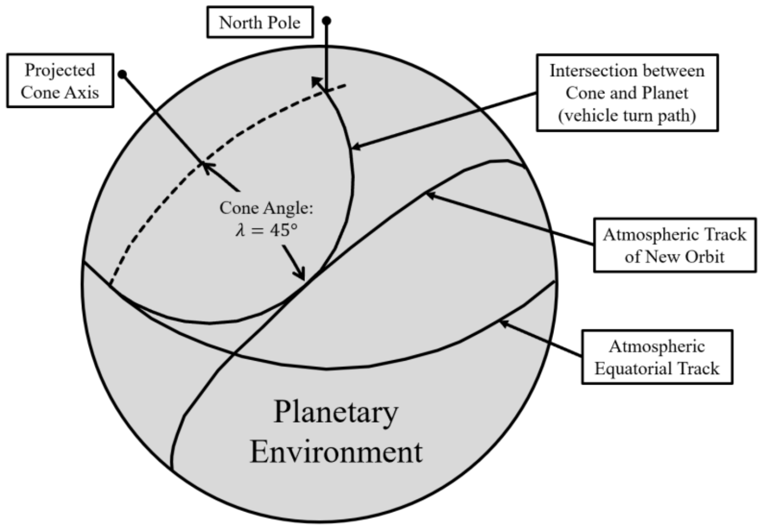

Figure 3.12: Synergetic Maneuver for a 45-degree Turn-Cone Angle

If the craft continues past this inclination change of 90 degrees, the new orbital inclination will lower, but in the opposite direction. For the purposes of the proposed missions, the author has reasoned that changing the orbital direction is not useful, as this can be decided by the starting conditions before the parking orbit. For these reasons, the maximum inclination for any craft will be 90 degrees. Any further geometric improvements towards increasing performance will garner no additional value to the performance index.

The user will now specify the importance of an inclination change. This can be important for a surprise reconnaissance mission as mentioned in the introduction. Additionally, the author will propose a mission to change inclination to rendezvous with an orbital station at a set inclination on another planet. Due to an initial inclination advantageous to a transfer orbit between the Earth and this planet, an inclination change would be required in orbit. This mission may limit the payload capability due to a necessary aerodynamic performance. In fact, higher aerodynamic performance may aid in reducing the required fuel to make the inclination change. Regardless, the performance of the synergetic maneuver is determined as follows, according to a user-specified weighting factor.

$$PI_{inc} = B_{PI}\frac{2(\Delta i)}{\pi}$$

Like the previous performance index, the performance variable Δi is normalized by the maximum value in radians. For a desired inclination, the B_{PI} must be set such that costs increase as a function of the maximum value. A good starting approximation for the weight can be defined by the desired inclination.

$$B_{PI} \approx \frac{\pi}{2(\Delta i)_{desired}}$$

The inclination change of a particular design is assessed according to $\Delta V_{available}$ and L/D. A proportion of the propellant is used to initiate descent for both one maneuver and the final descent, so multiple synergetic maneuvers incur that initial impulse cost.

The total inclination change is based on the turn angle achieved along the cone-sphere intersection circle with a cone angle of $\lambda = 45°$. The further the craft travels along this angle, the more velocity lost due to drag along this atmospheric circle. This velocity loss is determined by the range function denoted as $F(\bar{u}, \lambda)$. The full analysis, made by F. S. Nyland of the Rand Corporation, is found in reference [5].

The turn angle achieved is determined by tolerable velocity loss and the aerodynamic performance of the craft.

$$\varphi = \frac{1}{2}\frac{L}{D}[\ln|F(\bar{u}_i)| - \ln|F(\bar{u})|]$$

The range function based on velocity change is shown below.

$$F(\bar{u},\lambda) = 1 - \frac{\bar{u}^2}{(\sin\lambda)^2} - \frac{1}{\sin\lambda}\sqrt{\frac{\bar{u}^4}{(\sin\lambda)^2} - 2\bar{u}^2 + 1}$$

From these equations, the inclination change can be determined from the intersection cone and the turn angle achieved for each spacecraft.

$$\Delta i = \sin^{-1}\left[\sin\varphi\cos\lambda\sqrt{1 + \frac{1-\cos\varphi}{1+\cos\varphi}(\sin\lambda)^2}\right]$$

This analysis is implemented into the methodology and plotted for Earth values.

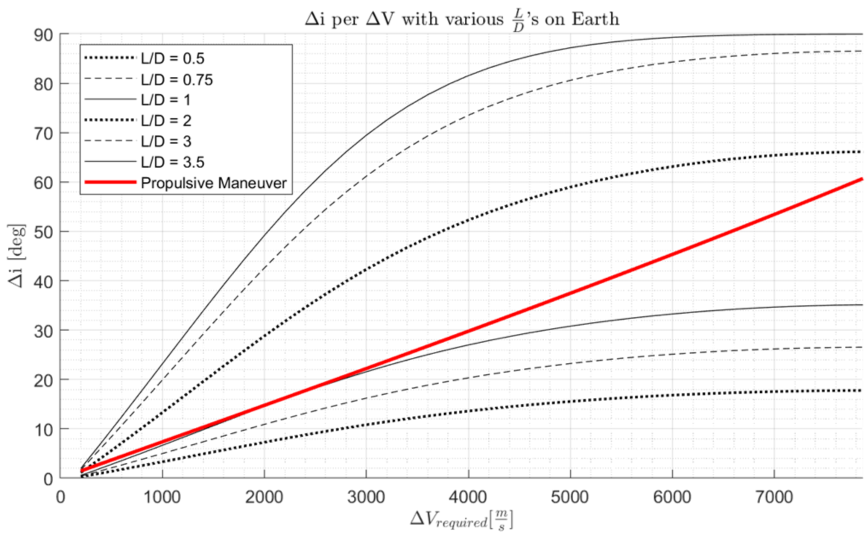

Figure 3.13: Lift-to-Drag Ratio Effect on Expended ΔV for an Earth Inclination Change

The code has been generalized to be applicable to any atmosphere with sufficient density. It is important to note that atmospheric models which are significantly less dense than that of Earth will compute an initiated turn below the planet's surface. However, even the atmosphere of Mars has an equivalent atmospheric density above its surface as the density used in Nyland's analysis.

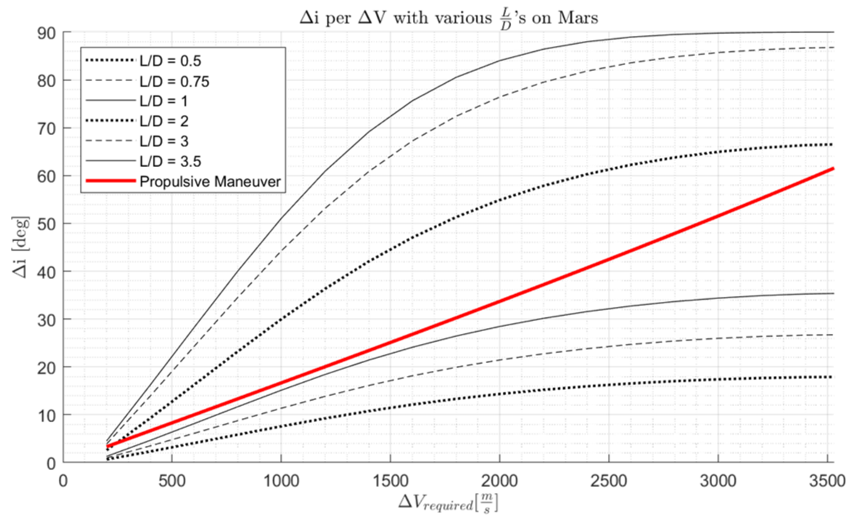

Figure 3.14: Synergetic Maneuvering Requirements on Mars

The requirements on a spacecraft orbiting 200 km above the Martian surface are significantly less than those required of initiating from a 200 km Earth orbit, but the comparison between a synergetic maneuver and a propulsive maneuver remains the same. It seems as though the inclination change requirements scale similarly with the planetary body (though not exactly the same, as variations between atmospheric heights require different periapsis altitudes for descent). In the Martian atmosphere, the turn is initiated at around 37 km above the surface, which is comparable to a turn initiation at about 64 km above sea level on Earth.

3.4.3 Descent Trajectory

The descent performance is assessed by three components, each with their own user-specified weights: cross-range, load factor, and heating. This is the only performance index component which itself contains multiple components. The effect of this is that these sub-components are less important if the performance index weights are equal. For this reason, if the mission calls for a descent component to be held at the equivalent value of a higher-level component such as inclination change, the performance weights must compensate for this. This hierarchy is more clearly demonstrated in the next subsection.

$$PI_{des} = C_{PI}\sqrt{\frac{\left(A_{des}\frac{s}{2\pi R_0}\right)^2 + \left(B_{des}\left|1-\frac{a_{load}}{10g_0}\right|\right)^2 + \left(C_{des}\left|1-\frac{\dot{q}}{\dot{q}_{max}}\right|\right)^2}{A_{des}^2 + B_{des}^2 + C_{des}^2}}$$

The cross-range of a spacecraft can be estimated by the lift-to-drag ratio and is later normalized by the planet's circumference. While a quick historical estimate is used below [7], the analysis found in reference [3] can provide more accurate and generalized cross-range analysis.

$$\text{Lateral Range [km]} = \text{LR}$$

$$= 0.539957\left[1.667 + 68.016\left(\frac{L}{D}\right) + 706.67\left(\frac{L}{D}\right)^2 - 91.111\left(\frac{L}{D}\right)^3\right]$$

$$\text{Down Range [km]} = \text{DR} = 0.539957 * 4866.6 + 4.70417(LR)$$

The range is plotted as a function of tau in Figure 3.15 as lift-to-drag can be estimated by this geometric parameter.

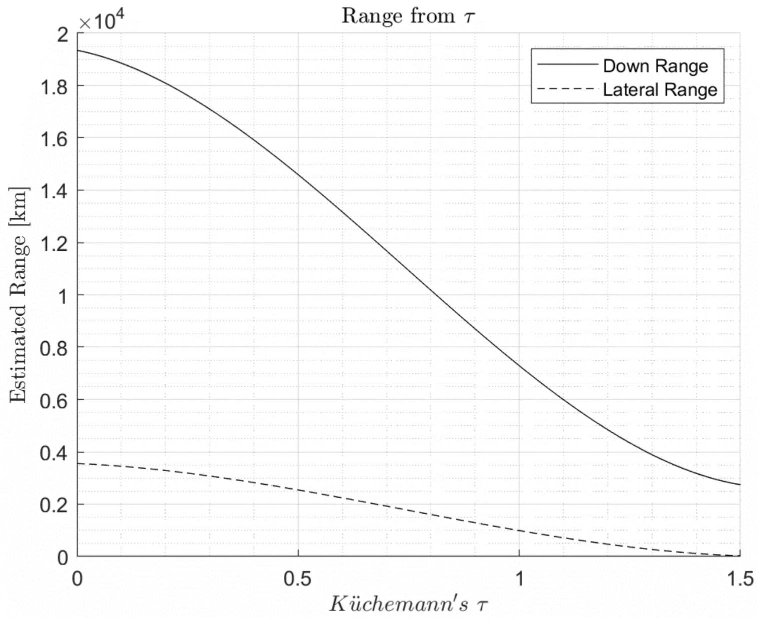

Figure 3.15: Vehicle Descent Range as a Function of Tau

The aerodynamic acceleration loading is dependent on the aircraft's basic aerodynamic characteristics and its current flight condition.

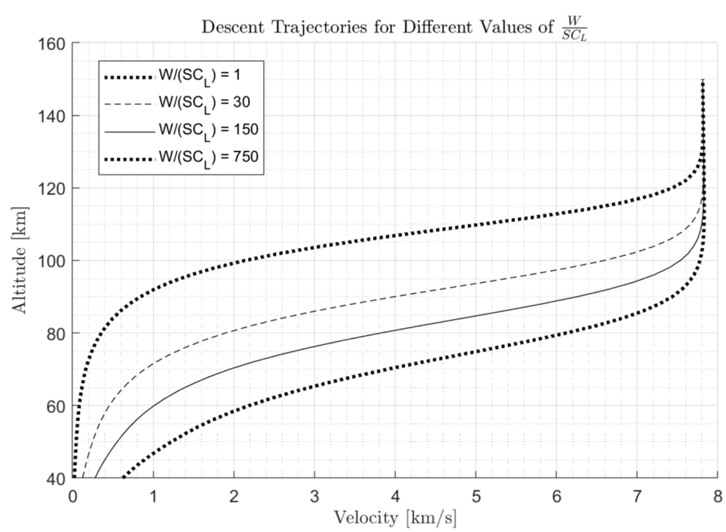

Figure 3.16: Steady Glides for Differing Vehicle Parameters

This flight condition is dependent on the point along a pre-determined steady glide as shown in Figure 3.16.

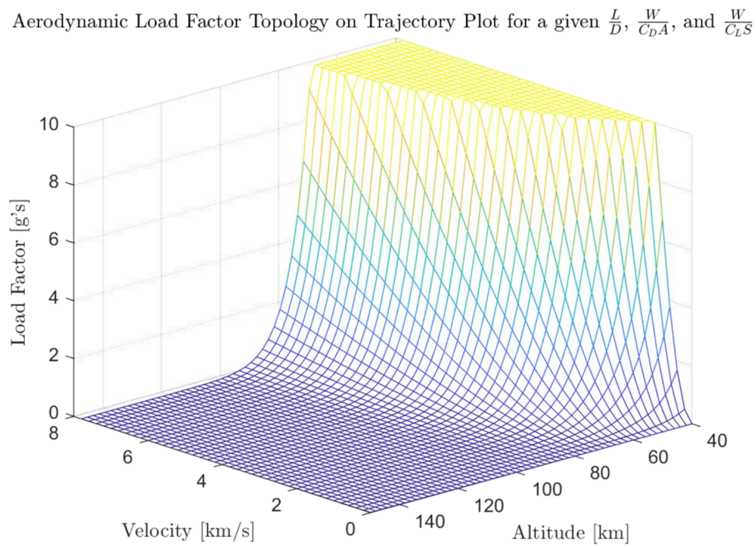

Figure 3.17: Aerodynamic Load Factor with Fixed Vehicle Parameters

Determining the maximum heating rate involves the same inputs as acceleration loading with the nose radius. This performance parameter is unique in that it is directly dependent on this one geometric parameter.

3.4.4 Total Performance

The vehicle must be assessed by a single parameter according to the weights selected by the user. These are normalized according to their maximum values.

$$PI_{tot} = \sqrt{\frac{\left(PI_{pay}\right)^2 + (PI_{inc})^2 + (PI_{des})^2}{A_{PI}^2 + B_{PI}^2 + C_{PI}^2}}$$

In summary, these performance indices are valued according to user preference in two hierarchy levels. This hierarchy is demonstrated with its associated user-specified weight in Figure 3.18.

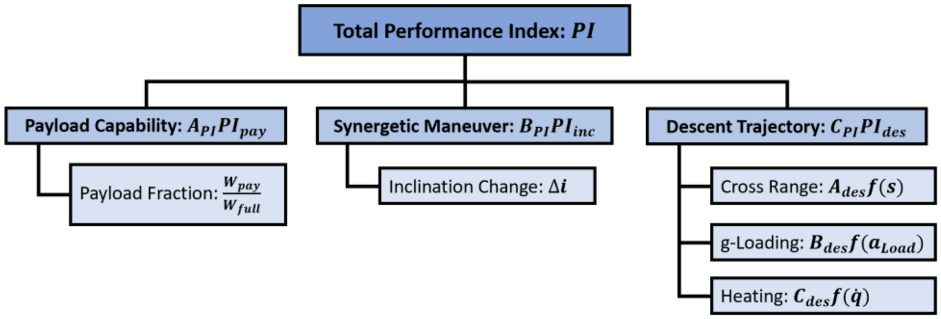

Figure 3.18: User-specified Weights define Mission Priorities

From here, the total performance index of any combination of the geometric parameters can be determined. By tweaking a geometric parameter, the user can view how this changes the performance. By this method an optimization routine can be applied to the methodology to see how a design can evolve to meet the mission requirements.

CHAPTER 4

APPLICATION

4.1 Code Architecture

4.1.1 User Settings

Assessing the performance of a spaceplane begins in the context of a planetary environment. The four parameters of a planetary environment (shown in Figure 4.1) are the first parameters loaded from a premade database of selected planets from reference [23] and a small set of hypothetical planets used to test the algorithm.

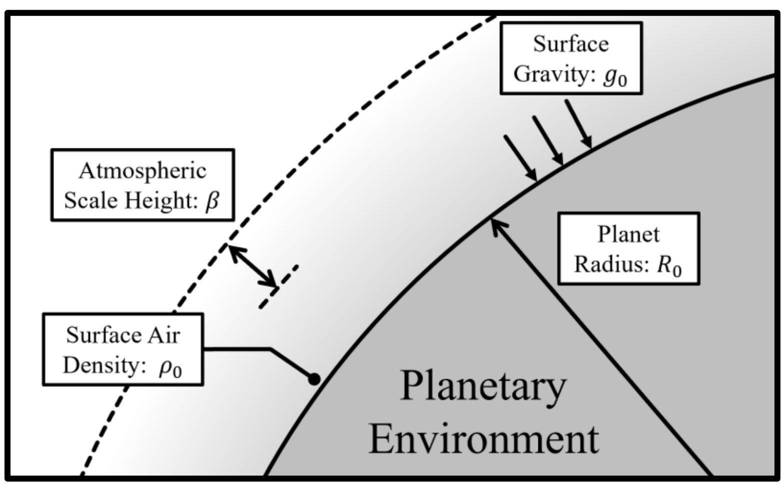

Figure 4.1: Four Parameters Describing the Planetary Environment

After a planet has been selected, the user adds a mission upon which the target spaceplane will be assessed. The mission is described by the weight and volume of the payload, the max g-loading to be endured by the payload, and the maximum heating rate to be endured by the craft. The last mission parameter is to be determined by the thermal protection system, but an estimate can be made based on current materials available.

Figure 4.2: Four Parameters Describing the Desired Mission

As discussed in the previous chapter, the performance weight settings are also tweaked so that each of the normalized performance components can be fairly compared and considered by the algorithm. In practice, the payload fraction must be weighted so that the payload mass-weight is comparable to the structural mass-weight. In this way, parameters which measure inclination change are on the same order of magnitude. Of course, this is dependent on user preferences as each program has a different budget and goals.

For optimization, the user will set a few learning parameters which will be discussed in a later section. Without optimization, these are all set to a default of one.

4.1.2 Assessment

Whether or not the configuration will be optimized, the algorithm takes a first guess or an existing configuration to assess. This is given in the order of the six geometric parameters presented at the beginning of the previous chapter. The five latter geometric parameters are input as being normalized the first (aft radius). In this way, during optimization, most of the parameters are not adjusted by their individual dimensions, but rather by their relation to the scale of the aft radius.

The performance is then assessed according to the mission and user-specified weights in the given planetary environment. The methodology for performance assessment is described in the previous chapter and encapsulated in a function.

During this assessment, a logic decides on the existence of a propulsion system depending on volume constraints. It also checks to see if the mission is viable. If not, performance values of zero will be output to let the algorithm know that the design is worthless in terms of meeting mission goals.

4.1.3 Full Process

The code architecture is documented in the Nassi-Schneiderman Diagram shown in Figure 4.3. The loops are ignored at the default optimization settings (where $i = j = 1$), so the main analysis for a point study can be summarized by the innermost loop process preceded by the initialization process.

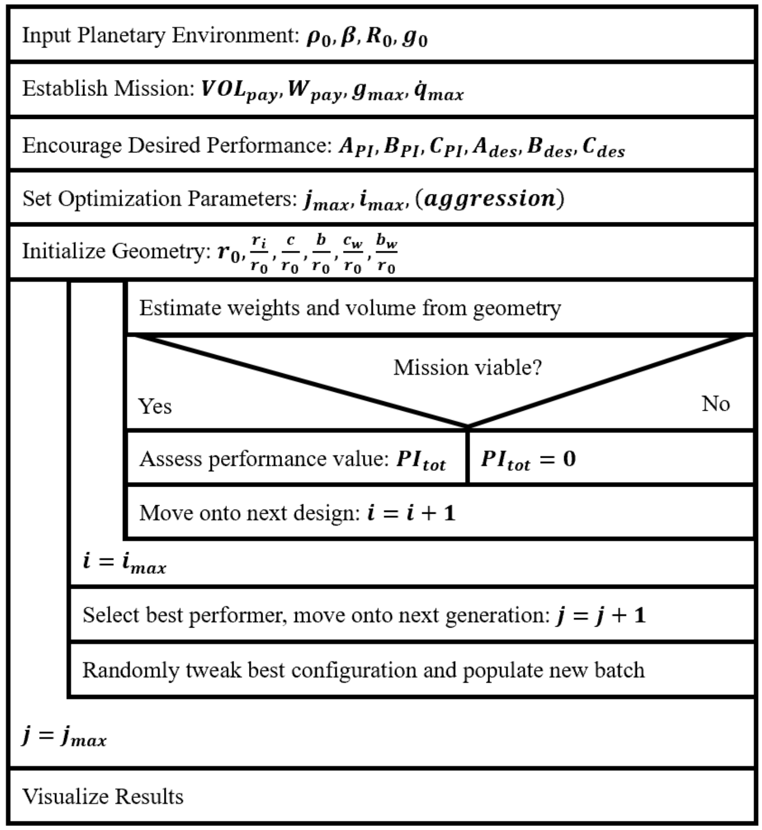

Figure 4.3: Nassi-Schneiderman Diagram of Code Architecture

4.2 Results and Comparisons

4.2.1 Trends in Geometry

The trends found in the geometric analysis are first analyzed. In keeping with trends for high-performing vehicles, the nose and aft radii are held fixed at $r_1 = 0.01r_0$. The wetted area can now by computed for varying values of chord and span, as shown in Figure 4.1.

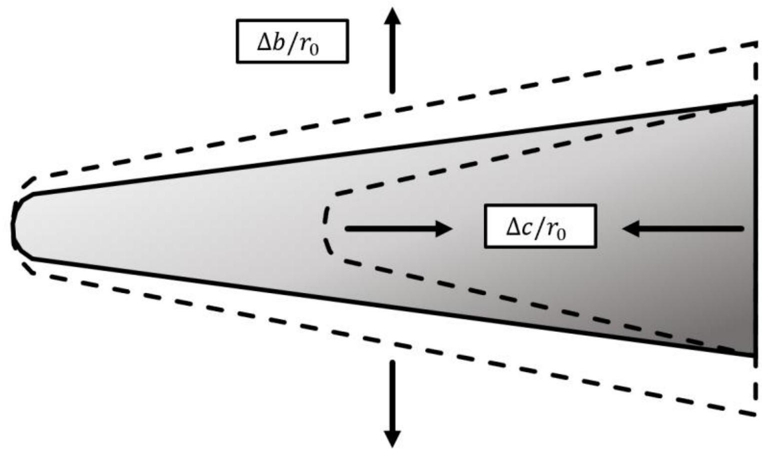

Figure 4.4: Adjusting Values of Chord and Span to View Trends

After setting bounds to the chord and span adjustment, the results for changing wetted area are shown in Figure 4.5.

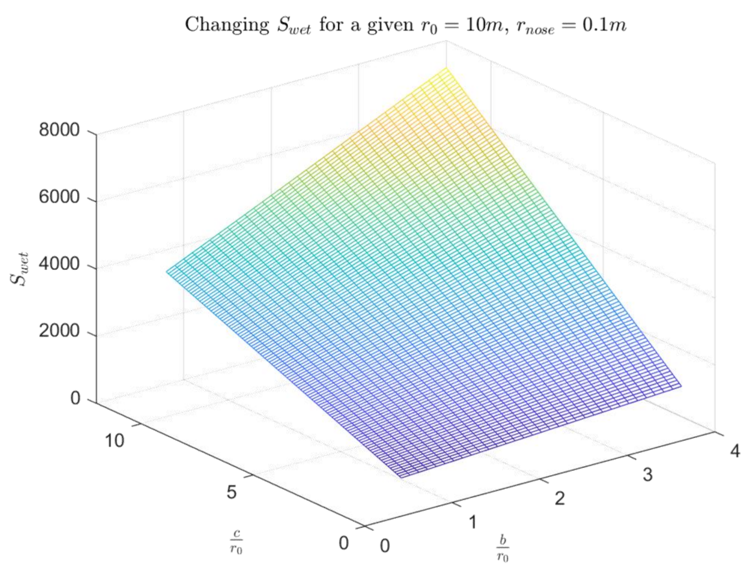

Figure 4.5: Wetted Area after Adjusting Span and Chord

The wetted area is the primary determinant of the structural weight, which is to be used in performance calculations. This changing structural weight is plotted in Figure 4.6.

$$W_{str} = I_{str} S_{wet} \text{ where } I_{str} = 17.1\ kg/m^2$$

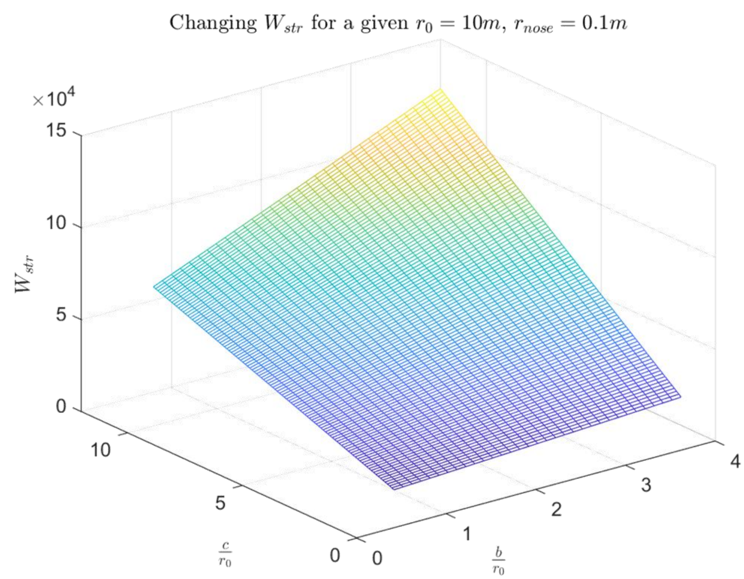

Figure 4.6: Structural Weight after Adjusting Span and Chord

The wetted area is the primary determinant of the structural weight, which is to be used in performance calculations. At the same time, Küchemann's Tau is competing with the structural weight. It is apparent by Figure 4.7 that the structural weight is inversely related to the tau parameter (take note that the x and y axes are inverted for the reader's visibility).

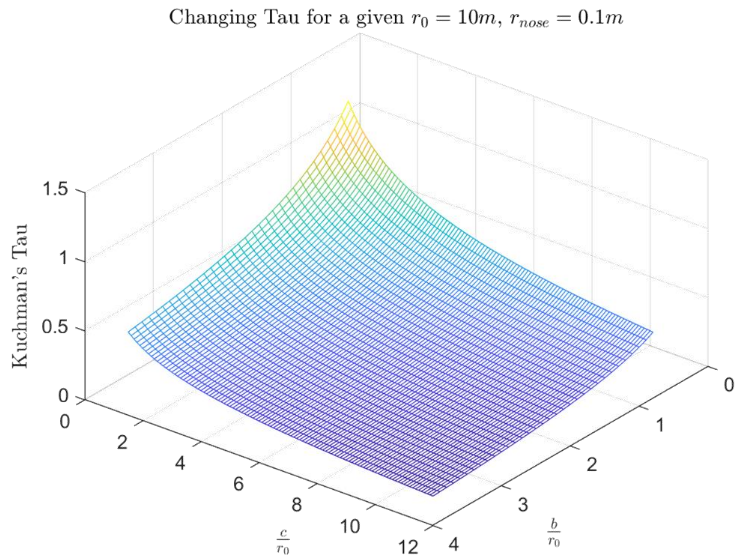

Figure 4.7: Küchemann's Tau after Adjusting Span and Chord

These two parameters must compromise with each other as the volume must remain fixed to meet the mission requirement and allow for a propulsion system with propellant if an inclination change is to be performed. The lowest Küchemann's Tau yields the highest lift-to-drag ratio and highest aerodynamic performance. The total configuration volume available for payload, propulsion system, and propellant is plotted in Figure 4.8.

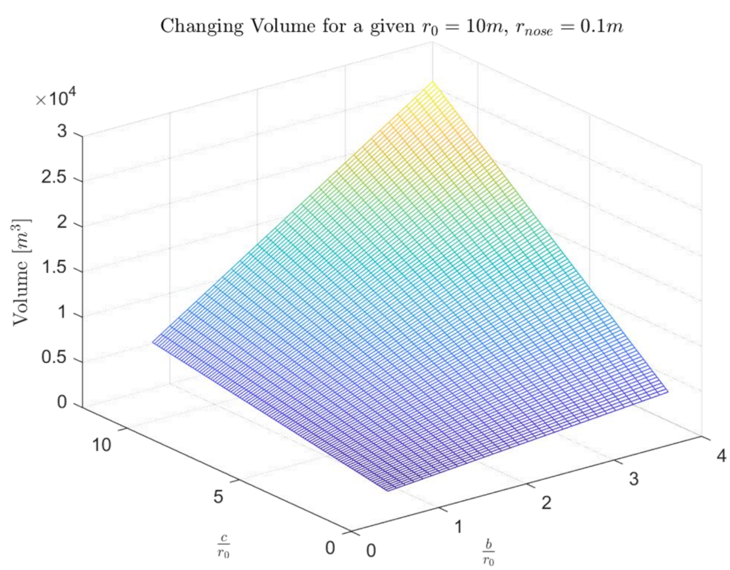

Figure 4.8: Available Volume after Adjusting Span and Chord

To see the full picture, the changing geometric results are now plotted for a changing nose radius. Of course, this is for a fixed chord and span so this plot can change along those dimensions, just as the 3-dimensional plots can changed along a third axis of nose radius size.

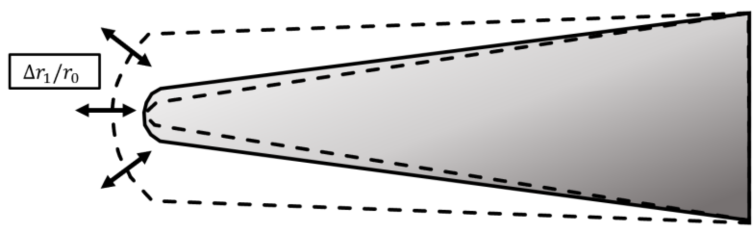

Figure 4.9: Adjusting Nose Radius to View Trends

Since only one parameter is being adjusted, the geometric analysis can be conducted on one plot with different lines separated by output category.

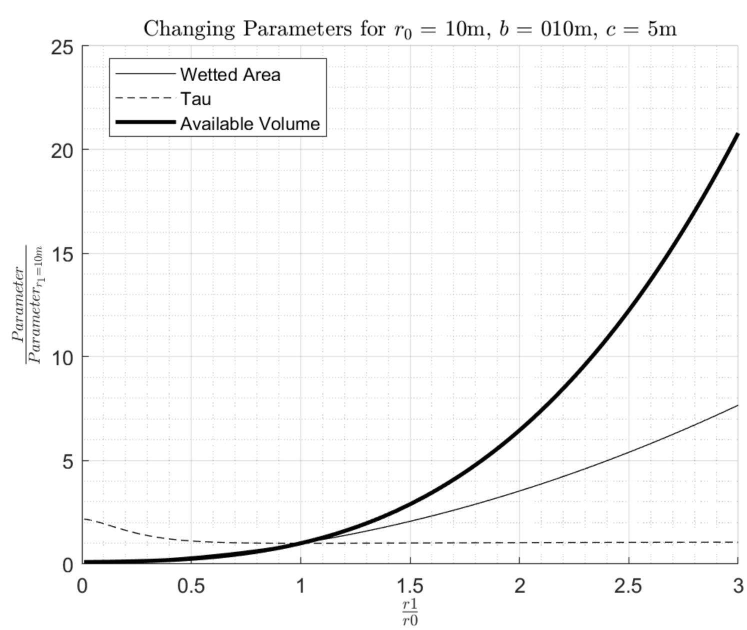

Figure 4.10: Changing Parameters after Adjusting Nose Radius

It is interesting to see that Küchemann's Tau is remaining roughly constant after the nose radius is about half of the aft radius. This is because tau is a function of shape, and once the nose increases past a certain point, the shape becomes dominated by the nose radius. Since the values are normalized, the trends for wetted area and structural weight are equivalent.

The author has observed that one of the most frequently changing parameters during optimization other than aft-radius scaling was the chord length in relation to the aft radius. The vehicle parameters are now observed for a changing chord length. An increase in chord length increases the available volume for propellant, decreases tau, but rapidly increases structural weight. Figure 4.11 shows the basic geometry parameters changing as a function of chord.

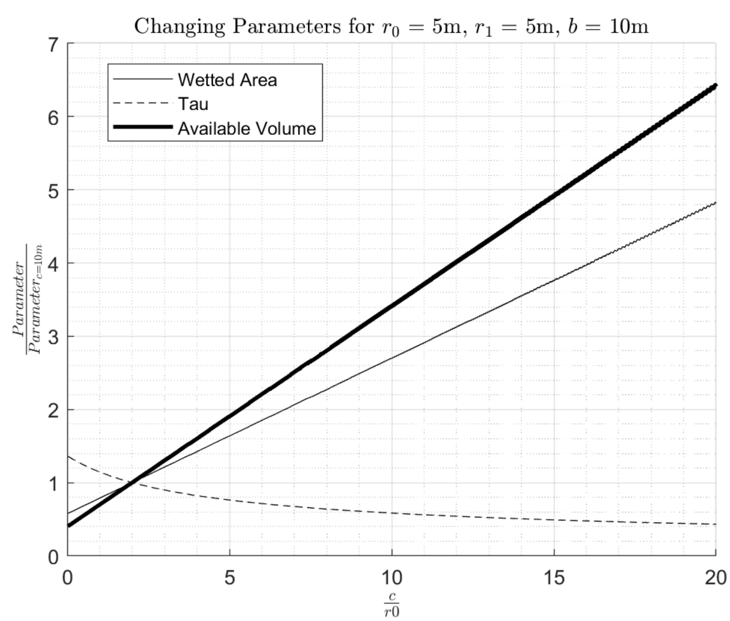

Figure 4.11: Changing Parameters after Adjusting Chord

Tau appears to be more well-behaved than when it was changing with respect to an ellipsoid shape expanding (increasing nose radius), and the wetted area and volume are increasing linearly as expected for a simple extrusion. Due to the radii being equal, this is equivalent to the "pill" shape expanding. The author arbitrarily selected this as the nominal condition, but any other combination of variables deviating from the nominal pill will also demonstrate a linear relationship in the same way that volume and area scales linearly with height regardless of cross section (for instance, stretching a cone would change its parameters linearly). Even with stretching, the change in tau is non-linear as it is a power relationship between two scaled heights. Additionally, it is unreasonable for tau to become negative by its definition, so one would expect its value to decay as a function of shape.

The inclination change capability of the vehicle is now assessed with respect to increasing chord in Figure 4.12, which is assessed for the planet Jupiter.

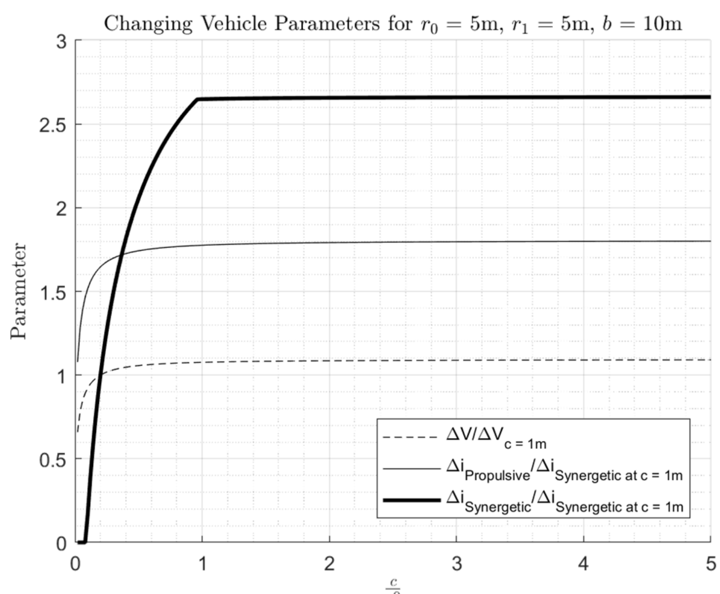

Figure 4.12: Inclination Change Capability with Increasing Chord

This is certainly a plot which proves the utility of a synergetic maneuver. Firstly, increasing chord length will increase $\Delta V_{available}$, but only up to a point. At this point, the increase in structural weight outweighs the benefit gained from increased value from gaining volume for propellant. This is why staging in a rocket greatly reduces the launch weight, since in a staged rocket, the velocity increment slope with increasing size is more of a steep linear line than a shallow asymptotic curve.

Given the $\Delta V_{available}$, an inclination change can be made in one of two ways: a synergetic maneuver (where aerodynamic capability comes into play) or a purely propulsive maneuver. It is shown that after a certain point with respect to the nominal value of a 1-meter chord, higher inclination change gains require employing the synergetic maneuver. Moreover, since the maximum $\Delta V_{available}$ is finite (with different finite values according to configuration constants), the change in inclination has a finite maximum, and only the synergetic maneuver can achieve the complete turn from an equatorial to a polar orbit.

4.2.2 Data Points

In this subsection some arbitrarily selected configurations will be assessed to build a database of initialization vectors for optimization.

The study will begin with assessing variations of the geometric trends with the categories of nose-to-aft ratios. It will then move on to superimposing wings, including an unrealistic low-sweep angle design which is not structurally feasible. However, this configuration will be useful for determining the bounds of the study.

- Big Nose
- Constant Nose

- Small Nose
- High Sweep Wing
- 45-degree sweep wing
- Low sweep wing

4.2.3 Historical Designs

This subsection will assess the accuracy of the performance assessment with real-world analogues. Correction factors and future analysis work will be discussed in the context of the findings. These designs can also serve as starting points (or target points) for optimization.

- Model 176
- Dream Chaser
- Dyna Soar Multi-Planet performance
- Space Shuttle
- Apollo 11 Capsule

4.3 Optimization

4.3.1 Methodology

The methodology for optimization begins with an initialized geometry vector, which represents any arbitrary configuration. The hope of optimization is that even a low-performing starting configuration will evolve into something realistic or useful after a given number of iterations.

The methodology of the optimization routine is inspired by the theory of biological evolution, where a design will be subjected to an environmental requirement and selective pressures, and only the best-performing designs will be allowed to have offspring. Of course, for the design to improve on learned attributes, the offspring of the best-performing configuration will resemble the parent. However, according to the aggressiveness of the learning rate, some of the children will be mutated in different ways. From here, the best performing child is assessed and used to populate the next generation. This process is visualized in Figure 4.13.

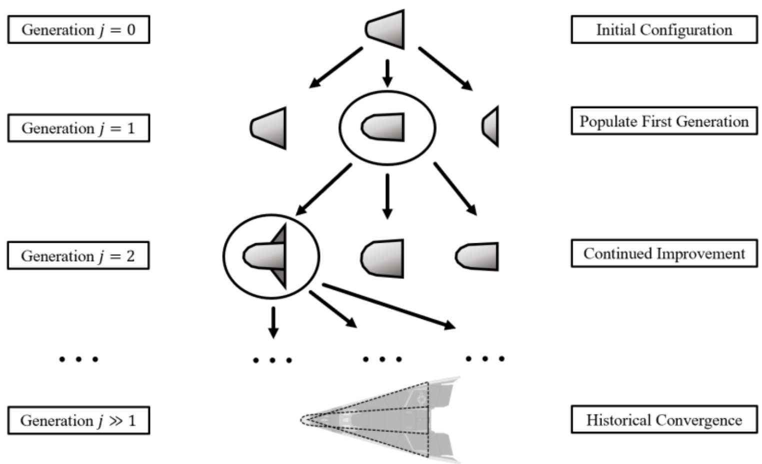

Figure 4.13: Genealogy of Configurations

As can be observed in Figure 4.13, the mutation function includes a small chance to spawn a wing. Conversely, a wing can be randomly removed. If a wing is detrimental to performance, its structural cost will cause children without it to be more successful than their peers.

Relating the evolution analogy to the mathematical reality, the optimization routine here is akin to a traveler along a multi-dimensional topology looking for a *local* minimum. Local minimums are numerous for these many parameters, which is why the screening of initialization values is necessary to find the best local minimum. The “mutations” are akin to small steps in random directions all at once in this topology. An increased number of children per generation relates to more steps in random directions per step, giving the traveler a better picture of where next to step. The aggressiveness of the mutations determines the size of these steps. Larger steps may converge on a solution faster, but it will increase the chance of divergence.

If all except two of the geometric parameters were held constant, the topology could be visualized in a 3-dimensional plot useful for visualizing the concept of the optimization routine (the topology shown in Figure 4.14 is from reference [24] for illustrative purposes and is not numerically representative of the actual topology produced by the author).

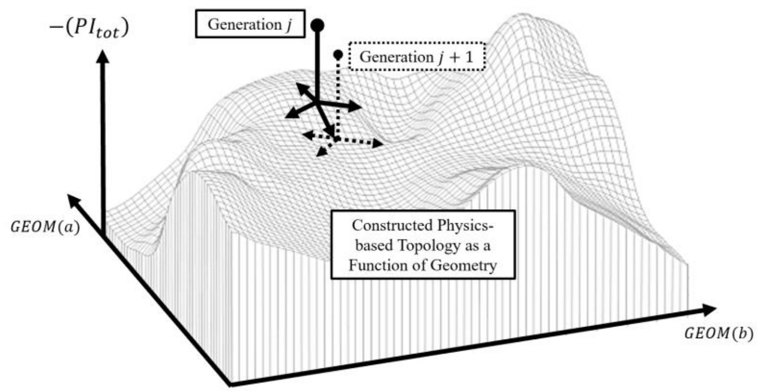

Figure 4.14: Topology Visualized in Optimization Routine

The number of steps taken per generation is analogous to the number of children per generation (this is the algorithm batch setting, with a default of $i = 1$). The best "step" is taken to the next generation. The number of non-trivial steps will always be less than or equal to the batch size, as not every offspring will mutate for low levels of aggression.

4.3.2 Results

The author initializes an early test of the algorithm with a non-sensical configuration employing a large nose and small wing. Evidently, the aerodynamics of such a craft are not efficient nor sized optimally for a mission with a payload of 100 kg and a volume of 10 m^3. The following figures show the top-view of the evolving configurations.

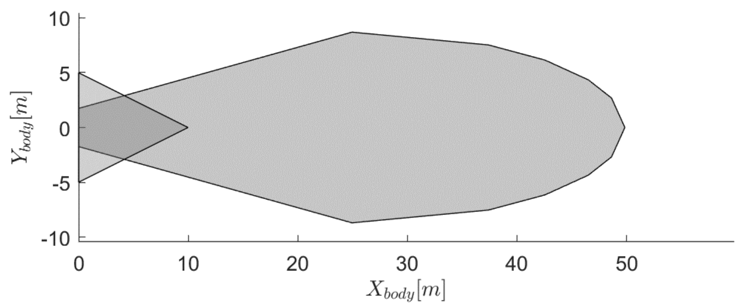

Figure 4.15: Generation 1 of First Successful Convergence

From here, the optimization routine takes small steps toward better-performing vehicles with each successive generation.

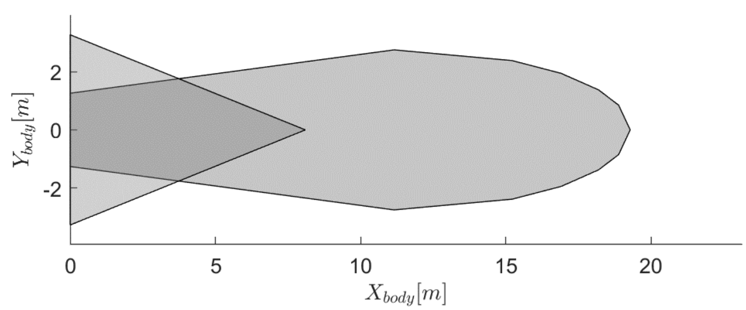

Figure 4.16: Generation 900 with Improved Performance

As shown by the axes of Figure 4.16, it is apparent that the most noticeably changed aspect of this configuration is the overall scale of the vehicle. This is due to the way the configuration's geometry vector is set up. The values are all with respect to element GEOM(1), which is the aft radius. Any change to this value will directly scale the rest of the design with it. In this way, the mutation function has an avenue of scaling the entire craft at once.

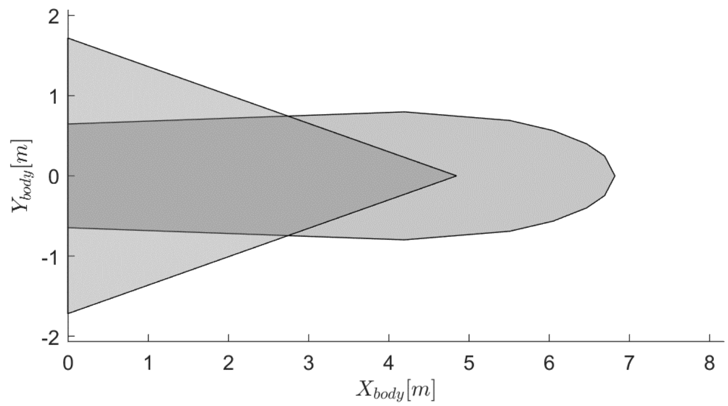

Figure 4.17: Generation 1600 with Improved Aerodynamic and Payload Capability

The configuration in Figure 4.17 is among the last with propulsive capability, as the weights were such that payload capability is increasingly favored over an inclination change. However, the $\Delta V_{available}$ for this configuration is 2.40 km/s with an engine achieving 350 seconds of specific impulse. Based on the aerodynamic capability of the Figure 4.17 configuration, the craft can only perform a propulsive inclination change. This is likely attributed to an inaccurate lift-to-drag estimation from a high tau value (which is a result of the desire to increase the payload fraction).

The key to a successful convergence is to find the correct costing function weights to teach the algorithm what the user is looking for. The first successful convergence had a very high payload fraction logic-weight, and resulted in the configuration seen in Figure 4.18.

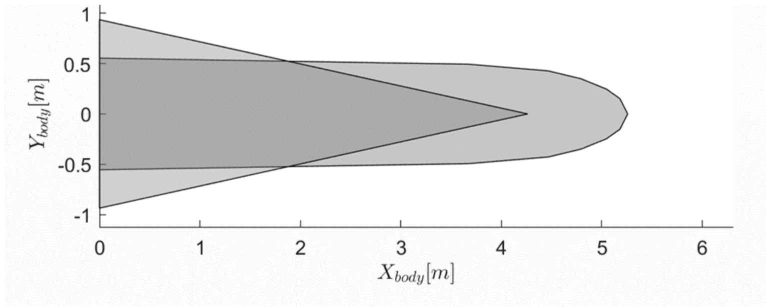

Figure 4.18: Generation 3000 Lacks Propulsive Capability to Increase Payload Capability

The conclusion of this first attempt was that there was too much emphasis placed on decreasing the structural weight. Such user-settings cause the algorithm to converge on a minimum-volume capsule design with residual wings. The geometric evolution and vehicle capabilities across these 3000 generations is plotted in Figures 4.19 and 4.20.

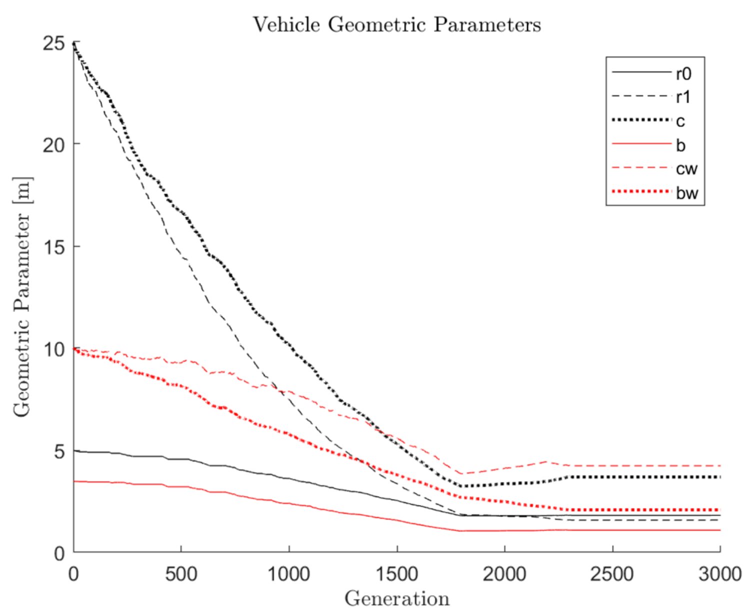

Figure 4.19: Vehicle Geometry Evolution for First Successful Convergence

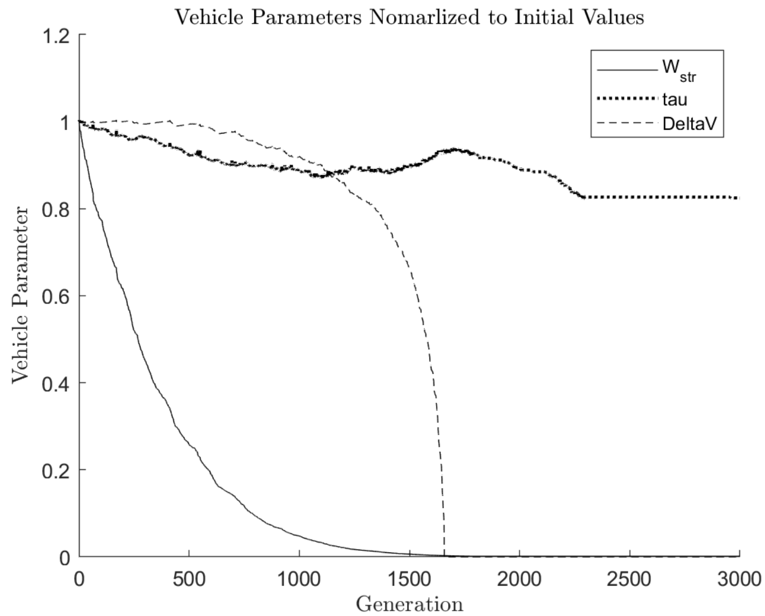

Figure 4.20: Vehicle Parameter Evolution for First Successful Convergence

In earlier unsuccessful convergence trials, the logic-weight for inclination change performance was set to dominate the logic-weight for payload fraction. This happens when the weights are equal to each other, as the payload fraction performance index tends to be very small due to the relationship between payload density at required structural weight to encapsulate it. Additionally, the density of the of the propellant will further exacerbate the trade-off between propulsive capability and payload capability. For these reasons, without a mission failure trigger, the algorithm will ignore the payload capability and focus on increasing the aerodynamic and propulsive capabilities. Fortunately, the model for estimating lift-to-drag has been set up to cap the performance to $L/D = 3$ according to conservative historical expectations [7]. As a result of this cap, the algorithm has little reason to continue slenderizing past the tau value associated with the L/D cap. It is worth noting that there is a minimum bound as well, which is why the Figure 4.17 configuration was assumed to be ballistic (obviously by observation, this estimation model must be modified to include low-performing configurations). After iterating using these weights the configuration converges to the configuration seen in Figure 4.21.

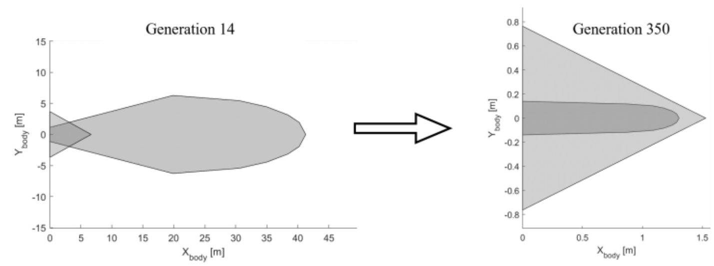

Figure 4.21: Convergence to Mission Failure where Aerodynamic Capability is too High

Using the alternative method of lift-to-drag estimation, the geometry converges to form a capsule shape.

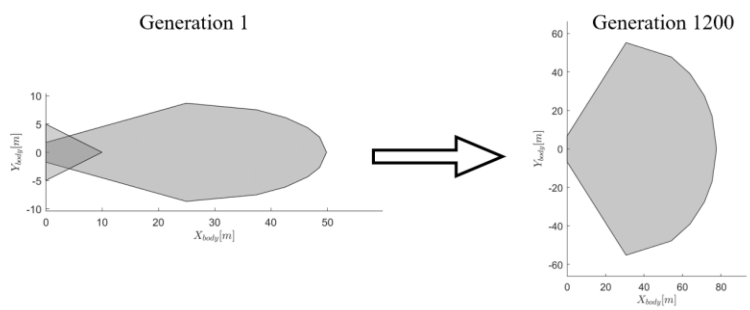

Figure 4.22: Convergence to a Capsule with Lifting Capability using New L/D Estimate

The geometric evolution of this lineage is shown in Figure 4.23. It converged in about half the time as the first convergence.

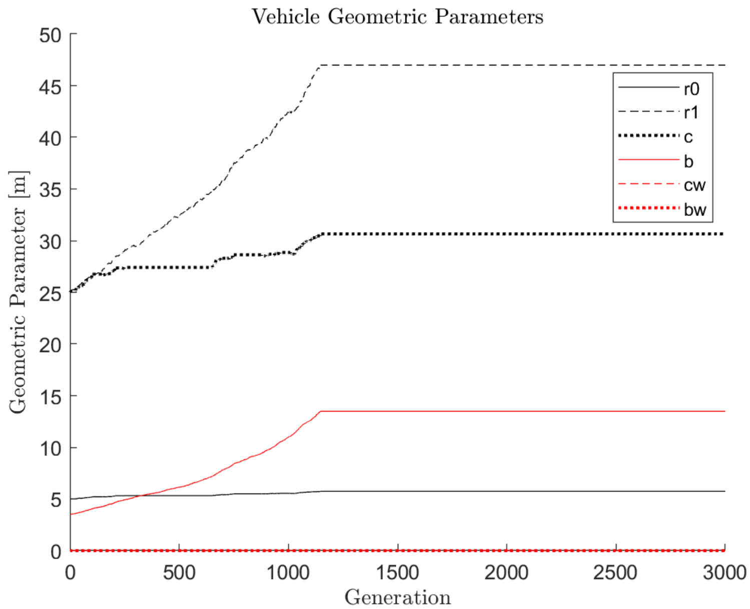

Figure 4.23: Geometric Evolution of Second Converged Configuration

The vehicle parameters in Figure 4.24 show that the velocity change available is relatively constant. The tau value changes in the same way that it would with an increasing nose radius.

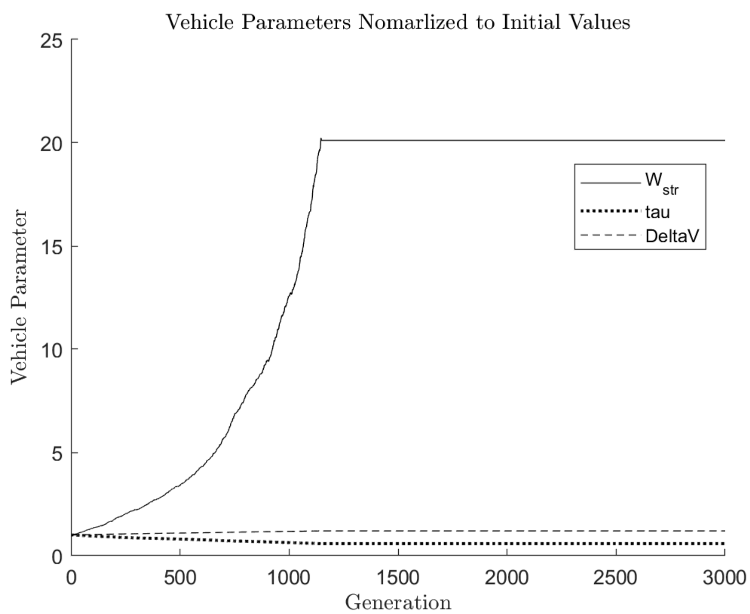

Figure 4.24: Vehicle Parameters in Second Converged Configuration

4.3.3 Observations

The algorithm exploited an earlier convergence attempt when the author neglected to factor in the nose section into the structural weight. While it did increase the loft section's wetted area, the growing nose area was not computed, so it became more advantageous to grow this section unrealistically.

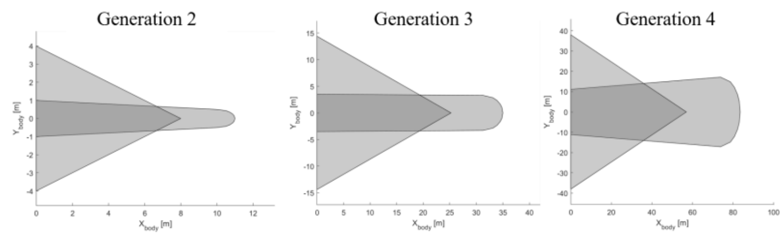

Figure 4.25: Growing Nose due to Structural Weight Calculation Mistake

CHAPTER 5

CONCLUSION

5.1 Concluding Remarks

This thesis has laid the groundwork for assessing the topology of re-entry vehicle configurations based on six geometric parameters. These parameters can approximate several historical designs, which can be assessed on this topology.

The performance analysis included assessing payload, inclination change capability (using both synergetic and propulsive mission profiles), and a descent analysis. The descent analysis had three main components: cross-range, g-loading, and heating. These performance parameters were then weighted by importance to converge on historical designs, where it was found that payload capability needed more of a weighting value to compensate for high structural weight. In this way, the weighting value here was related to the assumed structural index.

The optimization routine brought about several interesting observations, such as proof of the importance of the physical model. Whenever a solution was converged upon, this led to insight on the important variables to the model. The algorithm converged on an aircraft that eventually ignored lifting capability, favoring a minimum-volume design to reduce structural mass. This was the result of a high logic-weight on the payload fraction.

By the nature of the topic, there is much room for additional analysis to improve on the algorithm developed by the author. Some of the major points for improvement are discussed below.

5.2 Future Work

The work done in this thesis is only a foundation of a design methodology that will require more analysis methods to include more design considerations. For example, the most glaring hole in these analyses is that of determination of aircraft stability throughout the entire flight regime. A stable static margin was assumed since the delta wing starts at the aft chord endpoint, and the payload was assumed at the front of the spacecraft. More geometric parameters are required to ensure stability to factor into the "mission success" variable in the vehicle assessment function.

While this re-entry vehicle is analyzed for hypersonic aerodynamics, design for subsonic regimes are still required for advantageous operation. The author has assumed from literature that 8% of the structural weight was allocated to the decoupled mode, as applied to capsule conceptual design. However, assuming a decoupled mode does not utilize the high-lift capability of higher-performing designs.

The descent profile is somewhat disconnected from the geometric parameters, as assumptions were made to determine the lift and drag coefficients apart from merely the ratio between the two. However, the geometric analysis provides a starting point for computing these forces to generate vehicle parameters to accurately model the descent profile for a particular configuration. Future work should pay closer attention to the heating of the spacecraft, as this was not deeply covered in this thesis (thermal-protection system parameters assumed to be covered by the structural index).

The addition of planetary bodies other than earth are speculative, as no manned missions have been conducted in this environment at the time of this writing. In light of this, future work could possibly be written in a time where there is actually historical validation for the analysis conducted here. At this point, there could be a continuous link between the parameters of planetary bodies and their respective vehicle performances. In this case, some manned vehicles may have mission profiles requiring a configuration which is a compromise between two environments. This will require an extension of the optimization algorithm and a supplementing solution space generator.

APPENDIX A

NOMENCLATURE

Greek Letters:

β Atmospheric scale height [km]

γ Flight path angle [deg]

Δ Change in following variable, such as velocity

λ Minor cone angle for synergetic turn [deg]

ρ Mass density [kg/m^3]

τ Küchemann's Tau, $VOL/S_{plan}^{1.5}$

φ Turn angle [rad]

Subscripts:

0 Denotes initial or surface value

$\oplus$ Relating to planet Earth

θ Orientated along a curved surface in a polar coordinate system

C Of a circular orbit

des Relating to descent

D Drag

i Initial value for a differential equation, inclination, or batch ID number

j Generation ID number

PI Relating to performance index

req Variable defined by mission requirement

Latin Letters:

a Acceleration [m/s^2]

b Width or span [m]

A Reference area, perpendicular to aircraft centerline [m^2], logic-weight, or estimation constant

B Estimation constant, or logic-weight

c Chord length [m]

C Non-dimensional coefficient, or logic-weight

$Circ$ Circumference [m]

D Drag [N]

F Range function for synergetic turn

g Gravitational acceleration [m/s^2]

H Step size [m]

I_{sp} Engine Specific Impulse

I_{str} Structural Index [kg/m^2]

K Gravitational constant of a planetary body, $g_0 R_{earth}^2$

L Lift [N]

m mass [kg]

M Mach number

$\bar{M}$ Mean molecular mass [g/mol]

MR Mass Ratio, W_{full}/W_{empty}

N Integer count of that specified by subscript

p elliptical axis length 1 [m]

q elliptical axis length 2 [m]

$\dot{q}$ heating rate [J/ (m^2 s)]

r Local radius [m], [km]

R Universal Gas Constant [8.314 J/ (mol K)], constant planetary radius [m], [km]

s Path length as a planet surface ground-track [m], [km]

S Surface Area [m^2]

t Time [s]

$\bar{T}$ Mean temperature [K]

$\bar{u}$ Normalized ground track velocity

V Velocity [m/s], [km/s]

VOL Volume [m^3]

W Weight [N]

x Axial coordinate on aircraft configuration

y Altitude [m], [km], lateral coordinate on aircraft configuration

x vertical coordinate on aircraft configuration

Z Function Variable for Chapman's Trajectory Analysis [3]

REFERENCES

[1] J. P. Penn and C. A. Lindley, "RLV Design Optimization for Human Presence in Space," The Aerospace Corporation, El Segundo, California, 1997.

[2] G. Corning, Aerospace Vehicle Design, Ann Arbor: Braun-Brumfeild, 1964.

[3] D. R. Chapman, "An Approximate Analytical Method for Studying Entry into Planetary Atmospheres," National Advisory Comittee for Aeronautics (NACA), Washington, 1958.

[4] M. Sheetz and A. Macias, "President Trump directs Defense Department to 'immediately begin the process' of establishing 'space force' as sixth military branch," Consumer News and Business Channel (CNBC), 18 June 2018. [Online]. Available: https://www.cnbc.com/2018/06/18/president-trump-directs-pentagon-defense-department-to-immediately-being-the-process-of-establishing-space-force-as-sixth-military-branch.html. [Accessed 27 June 2018].

[5] F. S. Nyland, "The Synergetic Plane Change for Orbiting Aircraft," The Rand Corporation, Santa Monica, California, 162.

[6] L. Piñero-Pérez, "Design of Hypersonic Lifting Body Vehicle (Lead Chief Engineer's Report)," University of Texas at Arlington MAE Department, Arlington, 2018.

[7] P. A. Czysz, C. Bruno and B. Chudoba, Future Spacecraft Propulsion Systems and Integration, Berlin: Springer-Verlag, 2018.

[8] B. Chudoba, Interviewee, *MAE 4351 Lecture: Project Introduction.* [Interview]. 4 June 2018.

[9] J. Arizpe, "Design of Hypersonic Re-entry Vehicle (CAD/Performance Report)," University of Texas at Arlington MAE Department, Arlington, 2018.

[10] R. G. Hoey, Testing Lifting Bodies at Edwards, Palmdale: PAT Projects, 1994.

[11] North American Rockwell Corp. Space Division - Public Relations Department, "Apollo Spacecraft News Reference," North American Rockwell Corp., Downey, California, 1972.

[12] M. S. Agbabian, Lunar Missions and Exploration, New York: John Wiley & Sons, 1964.

[13] F. C. Grant, "Modulated Entry," NASA- Langley Research Center, Langley Field, Virginia, 1960.

[14] J. P. Duffy, Target: America: Hitler's Plan To Attack The United States, Santa Barbara, California: Lyons Press, 2012.

[15] D. Johnson, "Sanger," Luft '46, 9 July 2018. [Online]. Available: http://www.luft46.com/misc/sanger.html. [Accessed 1 August 2018].

[16] D. R. Reed, Wingless Flight: The Lifting Body Story, Washington D.C.: NASA History Office, 1991.

S. Sanz Fernández de Córdoba, "Fédération Aéronautique Internationale:

[17] Presentation of the Karman separation line, used as the boundary separating Aeronautics and Astronautics," 21 June 2004. [Online]. Available: https://www.webcitation.org/618QHms8h?url=http://www.fai.org/astronautics/100km.asp. [Accessed 1 July 2018].

[18] M. Brown, "X-20 Dyna Soar," Deviant Art, 13 September 2008. [Online]. Available: https://www.deviantart.com/bagera3005/art/X-20-Dyna-Soar-97785215. [Accessed 2 August 2018].

[19] NASA Content Administrator, "Project Mercury Explained," NASA, 7 August 2017. [Online]. Available: https://www.nasa.gov/multimedia/imagegallery/image_feature_1324.html. [Accessed 2 August 2018].

[20] Alphabet Inc., "Circumference of an Ellipse (Made Available by Search Query)," Google, 2018. [Online]. Available: https://www.google.com/search?q=circumference+of+ellipse&rlz=1C1SQJL_enUS788US788&oq=circumference+of&aqs=chrome.2.0j69i57j35i39j0l3.3284j1j7&sourceid=chrome&ie=UTF-8. [Accessed 2 August 2018].

[21] A. Ingenito, S. Gulli and C. Bruno, "Preliminary Sizing of an Hypersonic Airbreathing Airliner," *Transactions of the Japan Society for Aeronautical and Space Sciences, Aerospace Technology Japan,* no. January 2010, p. 19, 2010.

[22] P. Czysz and J. Vandenkerckhove, "Transatmospheric Launcher Sizing," *Progress in Aeronautics and Astronautics - Scramjet Propulsion*, vol. 189, pp. 979-1104, 2000.

[23] D. R. Williams, "Planetary Fact Sheet - Metric," NASA Goddard Space Flight Center, 18 July 2018. [Online]. Available: https://nssdc.gsfc.nasa.gov/planetary/factsheet/. [Accessed 4 August 2018].

[24] Polyhedron, "GINOSURF - The 3D/4D data display library for Contouring, Surface Mapping & X-Sections," Polyhedron - Software & Services, 2018. [Online]. Available: https://www.polyhedron.com/ginosurf. [Accessed 8 August 2018].

BIOGRAPHICAL INFORMATION

Leonardo Piñero-Pérez graduated with an Honors Bachelor of Science in Aerospace Engineering in August 2018. During his undergraduate education, he served as the President of the American Helicopter Society student chapter and functioned as the Treasurer of the American Institute of Aeronautics and Astronautics student chapter.

In his last semester, he conducted undergraduate research under Dr. David Hullender in non-Newtonian flow through an annular ring. This stems from Leonardo's Honors Senior Project finished in the previous semester, which involved designing an empirically-based control logic to maximize flow and pressure DC gains from an unknown, time-variant system such as a hydraulic fracturing well.

Leonardo has also worked as a teaching assistant for the computer-aided design class, writing the homework, creating design projects, and occasionally lecturing for the freshman and sophomore engineering class. He also has industry experience at Bell Flight, as a structural analyst supporting the MQ-8C Fire Scout Program. After graduation and a few backpacking trips, he will work with the flight controls team at Bell on future programs.

Leonardo's interests include flight controls, space vehicle design, and machine learning. He also enjoys backpacking, drawing, exercising, and reading philosophy.